Influence of Solution Composition and Temperature on the Strontium Content of Amorphous Calcium Carbonate and Subsequent Calcite

Adam M. Angel

Thesis submitted to the faculty of the Virginia Polytechnic Institute and State University in partial fulfillment of the requirements for the degree of

Master of Science
In
Geosciences

Patricia M. Dove
Donald J. Rimstidt
Benjamin C. Gill

July 19, 2013
Blacksburg, VA

Keywords: strontium, amorphous calcium carbonate, calcite, trace element distribution, non-classical mineralization, biomineralization

Influence of Solution Composition and Temperature on the Strontium Content of Amorphous Calcium Carbonate and Subsequent Calcite

Adam M. Angel

ABSTRACT

The Sr/Ca ratios in calcium carbonate fossils are used by the paleooceanographic community to infer past environmental conditions, such as sea surface temperature and ocean chemistry. The processes of biogenic calcification that produce these chemical signatures are complex and not fully understood, however, and vital effects are known to affect the trace element composition of the $CaCO_3$ biomineral products. The recent discovery that calcifying organisms produce amorphous calcium carbonate (ACC) as an intermediate phase during the crystallization process calls into question whether this pathway to mineral formation affects trace element distributions in the final product. This non-classical mineralization process raises the question of whether the Sr/Ca ratios of the final products are dependent upon temperature. That is, what is the temperature dependence of Sr/Ca ratios in calcite produced via ACC compared to the measurements obtained from calcite grown by the classical process in laboratory experiments and from biogenic settings.

The goal of this study is to determine the effects of solution chemistry and temperature on the Sr composition of ACC and resultant crystalline $CaCO_3$. Two types of experiments were designed: First, experiments were conducted to synthesize inorganic ACC in a batch reactor for a suite of selected chemical compositions and allowing this intermediate phase to transform into calcite in the reactant solution. In a second series of experiments, ACC was precipitated by a flow-through method to compare results to the batch reactor experiments. The experimental design focused on determining the Sr/Ca ratio and Sr distribution coefficients ($K_{D,\,Sr}$) of the amorphous and final crystalline products. Mg/Ca ratios of 5/1 were found to suppress Sr uptake into ACC by a factor of 25% when the initial Sr solution had concentration of one millimolar. ICP-AES data collected across the 18° to 30°C range showed that the Sr/Ca ratio in both ACC and the resultant calcite was independent of temperature. Upon transformation, the Sr/Ca ratios of both the ACC and calcite product were found to be similar, showing that Sr/Ca ratios were independent of the transformation process. Analysis of the data determined $K_{D,\,Sr}$ values of 0.564(±0.006) for ACC and 0.466(±0.009) for the resultant calcite in the 18-30°C temperature range.

The findings show that the Sr/Ca ratios of ACC and the transformed calcite are independent of temperature. However, the corresponding $K_{D,\,Sr}$ values exceed those reported for calcite grown by classical processes by an order of magnitude. The findings for the inorganic calcite yield $K_{D,\,Sr}$ values up to four times higher than those found in biogenic calcites. Because the findings of this study show that Sr/Ca is independent of temperature, this study calls into question whether previously reported Sr/Ca measurements in biogenic calcites should be revisited. It is plausible that biological

factors have a significant influence on trace element incorporation into biogenic calcite. Vital effects, such as the influence of macromolecules during the ion uptake process, may regulate the apparent Sr/Ca versus temperature trends observed in marine paleontology. Higher $K_{D, Sr}$ values in marine calcifiers may indicate that organisms use the non-classical mineralization pathway in whole or in part. Future studies of trace element incorporation in calcifying species should consider the pathway to mineralization in tandem with interpretations of environmental controls on distribution coefficients.

Table of Contents

List of Appendices

List of Figures

List of Tables

Introduction

1. Background

Paleoceanographic studies use a wide array of minor and trace element compositions in carbonates to infer past environmental conditions. Strontium can substitute for calcium in the calcite crystal structure as a trace element at levels that depend upon physiochemical conditions (Pingitore et al., 1992). For example, analyses of strontium concentrations in modern biogenic calcites show the Sr/Ca ratio correlates with sea surface temperature, salinity, pH (Lea et al., 1999), ocean depth (Elderfield et al., 1996), carbonate ion concentration (Russell et al., 2004), and pCO_2, (Dissard et al., 2010). Taking these variables into account, the correlation between Sr/Ca ratio and temperature can be compared to data in the fossil record to infer past environmental conditions (Stoll and Schrag, 1998).

The term "biogenic calcite" includes biologically produced carbonates in the skeletons of organisms. Generally, the trace element content of biogenic $CaCO_3$ depends upon the species of the calcifying organism and the polymorph of $CaCO_3$ that is mineralized. For example, the tests of modern species of planktonic and benthic calcite-bearing foraminifera show increases of 0.4(±0.002) Sr/Ca (mmol/mol) per 1°C change in seawater temperature (Russell et al., 2004). The shells of calcitic molluskan bivalves show a lower dependence with an increase of 0.014(±0.0054) Sr/Ca per 1°C, an order of magnitude lower than the foram observation (Wanamaker et al., 2008). In contrast, the Sr/Ca composition of other calcifying mollusk shells is not significantly correlated with temperature (Freitas et al., 2005). Each of these three trends in biogenic calcite differ

from Sr/Ca ratios measured in both inorganic aragonite and the biogenic aragonite of coral species, where Sr/Ca is reported to decrease by 0.038 per 1°C (Cohen et al., 2001).

These differences between trace element composition ratios are referred to as "vital effects", a qualitative term that loosely assigns differences in mineral compositions to biological factors. Taxonomic differences in trace element composition have long been recognized in biominerals (Weber and Raup, 1965). In addition, faster growth rates are also correlated with higher Sr content in marine organisms (Epstein et al., 1951, 1953). Daily fluctuations of light intensity affect growth rates in calcifying organisms, consequently influencing the trace element composition in the resultant biominerals (Cohen et al., 2001). It has been suggested that metabolic or kinetic effects influence the mineral composition (Lea et al., 1999). Although the significance of vital effects is well recognized and many studies have observed differences in element ratios across temperature in many taxa, the factors that regulate these variations are not fully understood and deter meaningful data interpretation.

2. ACC Background

The recent discovery that some marine calcifying organisms utilize amorphous calcium carbonate (ACC) during biomineralization (Beniash et al., 1997; Addadi et al., 2003) raises the question of whether the pathway to skeletal formation affects the trace element composition of the resultant crystalline phase. By this process, the organisms initially form a metastable amorphous phase ($CaCO_3 \bullet H_2O$) that later transforms into a crystalline product. Recent studies suggest that this particle-mediated growth results in an aggregation of nanoscale particles with grain boundaries in the transformed phase that

can be seen only at TEM resolution. A crystalline product with grain boundaries is defined as a mesocrystal, whereas a product without them is designated as a single crystal (Colfen and Antonetti, 2005). This type of mineralization, including the transformation process itself, is not well understood and is a subject of great interest in the geochemical community (Weiner et al., 2005).

A number of inorganic experiments have been conducted to investigate ACC composition and characterize the various products that crystallize upon transformation. Sand et al. (2012) showed that the concentration of alcohol in the reactant solution controls the polymorph of the resultant crystal. The Mg concentration that is present during formation affects the stability of the metastable ACC and slows the rate of transformation to calcite (Wang et al., 2012). A recent study shows that the distribution coefficient of Mg is dependent upon carbonate and hydroxide ion concentration (Blue et al., in press). Salinity has been suggested to affect ACC transformation and the composition of the solid products (Radha et al., 2010). Until the present study, no one has investigated the effects of trace element chemistry or temperature on the composition of ACC or the final product(s) that form upon transformation.

In marine calcifiers, ACC is reported in the spicules of sea urchins (Beniash et al., 1997) and mollusk larvae (Weiss et al., 2002). ACC has been identified as the first phase generated in bivalve shell and pearl growth (Jacob et al., 2008). It has been speculated that certain species of calcite-forming foraminifera utilize ACC via the "non-classical" mineralization pathway (de Nooijer et al., 2009). In terrestrial organisms, the presence of ACC is documented in isopods, where it is stored in the carapace and used in the molting process to form a crystalline shell (Zeigler, 1997). The presence of ACC in modern

marine organisms raises the question of whether ancient marine calcifiers utilized the ACC mineralization pathway and whether that process alters the Sr/Ca signature that is recorded in biogenic calcites.

To understand the empirical trends measured in this study, we begin by considering the general reaction for ACC formation in pure and Mg-Sr-bearing solutions. Gebauer et al. (2008) defines inorganic ACC formation by the following reaction:

$$z\mathrm{Ca}^{2+} + z\mathrm{CO}_3^{2-} = z(\mathrm{CaCO}_3)_{\mathrm{aq}} \cdot n\, H_2O \quad (1)$$

where *z* is the number of calcium carbonate units in a given ion pair or polymeric complex. The composition of ACC has been shown to have one or more waters of hydration and is included in Reaction (2) (Blue, in press; Wang, 2009). The absolute value of *z* is unknown, but assumes that the interaction of Ca^{2-} and CO_3^{2+} is stoichiometric. For the scenario where ACC forms in the presence of Mg and Sr ions, this general reaction can be expanded to reflect the formation of an amorphous Mg-Sr-$CaCO_3$ compound:

$$x\mathrm{Sr}^{2+} + y\mathrm{Mg}^{2+} + z\mathrm{Ca}^{2+} + (x+y+z)\mathrm{CO}_3^{2-} = (\mathrm{Sr_xMg_yCa_z(CO_3)_{x+y+z}})_{\mathrm{aq}} \cdot n\mathrm{H_2O} \quad (2)$$

where *x* is the number of $SrCO_3$ units in a cluster, *y* is the number of $MgCO_3$ units in a cluster, and the final solid solution has *x* plus *y* plus *z* units in the resultant cluster.

3. Distribution Background

The ratio of trace element concentrations between a solution and a calcium carbonate precipitate at equilibrium can be expressed as:

$$K_D = \left(\frac{m_{Tr}}{m_{Ca}}\right)_{solid} \Big/ \left(\frac{m_{Tr}}{m_{Ca}}\right)_{solution} \quad (3)$$

where K_D is the distribution coefficient, *Tr* is the subject trace element, and *m* is the molar concentration of an element in either the solid product or final solution. For the conditions where Sr is the impurity, equation (3) predicts a linear relationship between the Sr/Ca ratios of ACC or calcite with respect to their steady states.

$K_{D,\,Sr}$ for inorganic calcite has been extensively studied using various methods and a wide range of chemical conditions. Each of these studies was based upon the assumption that calcite growth occurred by the classical crystal process of ion-by-ion attachment to propagating steps of a crystal surface. Early experiments were performed by carbon dioxide pressurization at high temperatures (Holland et al., 1964). Other high temperature experiments involved synthesized aragonites transformed to calcite in sodium carbonate and sodium bicarbonate solutions (Katz et al., 1972; Malone and Baker, 1999). Experiments performed at temperatures relevant to biological conditions were conducted using batch reaction methods where calcite formed by precipitation or seeded growth (Kitano et al., 1971; Lorens, 1981). Mucci and Morse (1983) performed a calcite seeding experiment in synthetic seawater at environmental temperatures. ACC was not an intermediate in these experiments. A summary of these studies in Tables 1 and 2 shows the specific conditions of the experiments.

A closer look at K_D values reported by studies based upon data from live culturing and field investigations (Tables 1 and 2) show that distribution coefficients in calcifying marine organisms are similar to those measured in inorganic calcite experiments, with $K_{D,Sr}$ values of approximately 0.02-0.14. The $K_{D,\,Sr}$ values determined for Pleistocene benthic forams are similar to those of inorganic experiments (Bender et al., 1975) with

Table 1: List of strontium distribution coefficients for biogenic and inorganic calcite.

Reference	Method	Experimental Conditions	T (°C)	$K_{D, Sr}$	λ_{Sr}
Laboratory or inorganic experiments					
Holland, 1964	carbon dioxide pressurization	Ca, ammonium hydroxide solution	90-100	0.076	
Kitano et al., 1971	batch reaction	Ca, Mg, sodium citrate solution; week-month mixing	20		0.08
Katz et al., 1972	aragonite to calcite transformation	Ca, sodium carbonate solution; up to 100 days residence time	40-98	0.034-0.039	0.055-0.059
Lorens, 1981	calcite seeding	NaCl, Ca, sodium bicarbonate solution; pH=7.34-7.5	25	0.027	0.027
Mucci and Morse, 1983	calcite seeding	synthetic seawater, ionic strength = 0.697 M; carbon dioxide bubbling; pH=7.5-8	25	0.146	
Malone and Baker, 1999	aragonite to calcite transformation	Ca, sodium bicarbonate solution; ionic strength = 0.86 M; pH=7.5	40-200	0.046-0.071	
Angel (this study)	ACC formed via batch reactor	batch reaction of salt reagents and $NaHCO_3$, Mg/Ca = 5/1, [Sr]=0.1-1.0 mM, mixing pH = 8	18-30	0.54± 0.006*	0.66± 0.006*
Angel (this study)	ACC formed via flow-through reactor	flow-through reaction of salt reagents and $NaHCO_3$, Mg/Ca=5/1, [Sr]=0.1-1.0 mM, mixing pH = 8	25	0.79± 0.089*	
Angel (this study)	calcite via ACC precursor	transformation of ACC in solution; Mg/Ca = 5/1, [Sr]=0.1-1.0 mM, pH=7.5	18-30	0.46± 0.009*	0.60± 0.008*
Reference	Species	Investigative Conditions	T (°C)	$K_{D, Sr}$	λ_{Sr}
Live culturing or field studies					
Bender et al., 1975	*G. ruber* and *G. sacculifer*, foraminifera	Upper Pleistocene sediments, Tasman Sea; North Atlantic core tops; high-Mg calcite	21-29	0.16	
Lorens and Bender, 1980	*M. edulis*, bivalve	Cultured in filtered, Mg-adjusted seawater; low-Mg calcite	22-24	0.13	
Elderfield et al., 1996	*C. wuellerstorfi*, foraminifera	Global core top and benthic collection; ocean depth up to 5 km; high-Mg calcite	10-25	0.143-0.177	
Rosenthal et al., 1997	*Cibicidoides* species, foraminifera	Box core collection, Little Bahama Bank, ocean depth up to 1.6 km; high-Mg calcite	5-18	0.15-0.18	
Lorrain et al., 2005	*P. maximus*, bivalve	Seafloor dredging, Bay of Brest, ocean depth of 30 m; high-Mg calcite	10-18	0.20	

** - Statistically calculated average across conditions. Refer to Tables 4 and 5 and Fig. 13 and 14 for conditions of individual experiments.*

Table 2: List of magnesium distribution coefficients for biogenic and inorganic calcite.

Reference	Method	Experimental Conditions	T (°C)	$K_{D, Mg}$	λ_{Mg}
Laboratory or inorganic experiments					
Katz et al., 1973	aragonite to calcite transformation	Ca, sodium carbonate solution; up to 100 days residence time	25-90	0.059-0.187	0.057-0.116
Mucci and Morse, 1983	calcite seeding	synthetic seawater, ionic strength = 0.697 M; carbon dioxide bubbling; pH=7.5-8	25	0.0123	
Oomori et al., 1987	batch reaction	Ca, Mg, calcium bicarbonate solution; CO_2 gas bubbling	10-50		0.012-0.040
Angel (this study)	ACC formed via batch reactor	batch reaction of salt reagents and $NaHCO_3$, Mg/Ca = 5/1, [Sr]=0.1-1.0 mM, mixing pH = 8	18-30	0.056± 0.0009*	0.017± 0.0012*
Angel (this study)	ACC formed via flow-through reactor	flow-through reaction of salt reagents and $NaHCO_3$, Mg/Ca=5/1, [Sr]=0.1-1.0 mM, mixing pH = 8	25	0.787± 0.089*	
Angel (this study)	calcite via ACC precursor	transformation of ACC in solution; Mg/Ca = 5/1, [Sr]=0.1-1.0 mM, pH=7.5	18-30	0.023±0.0004*	0.094± 0.0011*
Reference	Species	Investigative Conditions	T (°C)	$K_{D, Mg}$	λ_{Mg}
Live culturing or field studies					
Rosenthal et al., 1997	*Cibicidoides* species, foraminifera	Box core collection, Little Bahama Bank, ocean depth up to 1.6 km; high-Mg calcite	5-18	0.02-0.06	
Wansard et al., 1998	*Candona* species, ostracods	Lacustrine core top and benthic collection; water depth up to 11 m; high-Mg calcite	10-21	0.005-0.0198	
Hiebenthal, 2009	*M. edulis*, bivalve	Cultured in filtered, Mg and Sr-adjusted seawater; low-Mg calcite	4-25	0.0006-0.0032	

** - Statistically calculated average across conditions. Refer to Tables 4 and 5 and Fig. 15 and 16 for conditions of individual experiments.*

$K_{D,\,Sr}$ = 0.16. Modern foraminifera acquired from core top samples and benthic dredging (Elderfield et al., 1996; Rosenthal et al., 1997), as well as shells of bivalves (Lorrain et al., 2005), have distribution coefficients similar to the Pleistocene forams. Calcite-bearing bivalve cultures in seawater that had been adjusted for Mg content also showed a similar $K_{D,\,Sr}$ value (Lorens and Bender, 1980). Stoll et al. (2002) determined in a coccolith culturing study that $K_{D,\,Sr}$ had a positive correlation with calcification rate, with $K_{D,\,Sr}$ = 0.275-0.376. Both the inorganic and biological distribution coefficients provide a background for comparing the $K_{D,\,Sr}$ value in both ACC and the resultant crystal.

4. Doerner-Hoskins Analysis of λ_{Sr} and λ_{Mg} in ACC

Because the Sr/Ca and Mg/Ca ratios in the solution increase as ACC precipitates, calculating the partition coefficient (λ) can determine the partitioning of a trace element into a solid by taking into account only the initial solution and final solution chemistry. The model expresses λ as:

$$\lambda = \ln\left(\frac{m_{Tr}}{m_{Tr}^{o}}\right) / \ln\left(\frac{m_{Ca}}{m_{Ca}^{o}}\right) \quad (4)$$

where m is the total concentration of an element in the final solution and m^o is the total concentration of element in the initial solution, expressed in moles. Therefore, $\left(\frac{m_{Tr}}{m_{Tr}^{o}}\right)$ represents the ratio of trace element in final solution over inital solution, and $\left(\frac{m_{Ca}}{m_{Ca}^{o}}\right)$ represents the ratio of calcium in final solution over initial solution (Doerner and Hoskins, 1925).

A comparison of distribution and partition coefficients from this study and other experimental studies is shown in Tables 1 and 2. Note that the Doerner-Hoskins approach does not use an analysis of the solid product. Furthermore, the Doerner-Hoskins model is

not utilized in field investigations and live culturing studies because the final solution chemistry is difficult, if not impossible, to constrain for the fossil or creature in question. Analysis of the solid ACC and calcite in this study allows for comparison to other studies where the solid product is explicitly used to calculate trace element distribution (see Tables 1 and 2).

The summary of previous studies (Table 1) shows strontium distribution coefficients are related to the assumed classical terrace-ledge-kink mineralization pathway (Kossel, 1927), regardless of whether the investigation involves inorganic precipitation or biological growth. Determining the distribution of trace elements in ACC is needed to further understand whether mineralization pathway influences the final calcite composition. Furthermore, measuring the effect of ACC transformation on strontium composition without biological influence provides an important inorganic baseline for comparisons to organic effects. Establishing this baseline is critical to better understand and quantify the effect of mineralization processes on crystal composition. This goal of this project was to evaluate the influence of solution composition and temperature on the Sr content of ACC and resultant calcite that forms. I hypothesize a lower Sr/Ca ratio and a lower $K_{D,\,Sr}$ in the resultant calcite due to the decrease in phase solubility after the transformation of ACC.

Materials and Methods

1. Synthesis Using a Batch Reactor

a. ACC formation

Reagents of $CaCl_2 \bullet 2H_2O$ (SigmaAldrich, >99%), $MgCl_2 \bullet 6H_2O$ (SigmaAldrich, >99%), and $SrCl_2 \bullet 6H_2O$ (SigmaAldrich, 99%) were prepared to obtain the proper cation concentrations upon mixing. All experiments used a Ca^{2+} concentration of 25 mM; Mg^{2+} concentrations were set to obtain ratios of Mg/Ca equal to 1.0, 2.0, and 5.0 mol/mol; and Sr^{2+} concentrations were set to 0.1, 0.5, and 1.0 mM. These solutions were then stored in an incubator until they reached the temperatures used for the experiments (18°C, 22°C, 25°C, and 30°C). The solution concentrations used in this study are summarized in Table 3.

Amorphous calcium carbonate was synthesized by modifying the batch reaction method of Glover and Sippel (1967). This procedure mixes the solutions in a closed system to form a precipitate, which is then separated from the solution. The final solution and the solid precipitate are then analyzed to determine the Sr/Ca concentration values.

To conduct a synthesis, 100 mL of 100 mM sodium bicarbonate (SigmaAldrich, >99%) solution was prepared immediately before batch mixing and allowed to reach the desired temperature. The initial pH of the $NaHCO_3$ solution was adjusted to 9.5 by adding 5 milliliters of 1.0 molar NaOH. The bicarbonate solution was poured into the cation reagent in a 250 mL jar and mixed under stirring for two minutes. The ACC formed immediately as a cloudy white precipitate. The pH of the solution was immediately measured upon mixing. A 25 mL aliquot, containing ACC precipitate and solution, was collected two minutes after initial mixing. The jar was removed from

Table 3: Summary of experimental conditions for batch reactor and flow-through reactor experiments with Sr/Ca ratios of the ACC that was produced. Each experiment was performed at 25°C and an initial $CaCl_2$ concentration of 25 mM. Batch reactor data is from the extraction at 45 minutes.

Batch Reactor

Initial Solution Chemistry		Reaction Chemistry							
[Mg] (mM)	[Sr] (mM)	Mg/Ca soln	Sr/Ca soln	Mg/Ca ACC	Sr/Ca ACC	$K_{D,Mg}$	$K_{D,Sr}$	λ_{Mg}	λ_{Sr}
25	0.1	27.15	0.005	1.93	0.004	0.071	0.774	0.057	0.955
25	0.5	10.05	0.026	0.63	0.016	0.063	0.626	0.076	0.894
25	1.0	6.34	0.056	0.35	0.032	0.055	0.573	0.094	0.833
50	0.1	18.9	0.005	1.24	0.003	0.066	0.689	0.046	0.930
50	0.5	14.3	0.024	0.83	0.015	0.058	0.657	0.057	0.921
50	1.0	18.3	0.045	0.99	0.030	0.054	0.649	0.056	0.945
125	0.1	8.82	0.006	0.60	0.003	0.073	0.584	0.047	0.518
125	0.5	8.85	0.025	0.50	0.014	0.053	0.576	0.091	0.680
125	1.0	8.94	0.051	0.51	0.027	0.058	0.530	0.044	0.605

Flow-Through Reactor

Initial Solution Chemistry		Reaction Chemistry							
[Mg] (mM)	[Sr] (mM)	Mg/Ca soln	Sr/Ca soln	Mg/Ca ACC	Sr/Ca ACC	$K_{D,Mg}$	$K_{D,Sr}$	λ_{Mg}	λ_{Sr}
25	0.1	5.35	0.008	0.139	0.004	0.026	0.463	0.222	0.869
25	0.5	6.47	0.072	0.168	0.017	0.013	0.882	0.360	0.562
25	1.0	1.30	0.042	0.034	0.033	0.043	1.071	0.317	0.985
50	0.1	2.62	0.004	0.068	0.004	0.020	0.239	0.315	0.970
50	0.5	2.78	0.016	0.072	0.016	0.014	0.909	0.304	1.054
50	1.0	4.08	0.031	0.106	0.033	0.055	0.987	0.274	1.064
125	0.1	4.99	0.004	0.130	0.004	0.098	0.788	0.326	1.014
125	0.5	3.80	0.017	0.099	0.015	0.095	0.937	0.361	1.057
125	1.0	11.09	0.041	0.288	0.029	0.195	0.806	0.600	0.984

stirring, resealed, and returned to the incubator. A second 25 mL aliquot was collected 45 minutes after initial mixing.

The 25 mL aliquots were centrifuged for 15 minutes at 10,000 rpm at the experimental temperature, separating the ACC from the aqueous phase. Five milliliters of supernatant was removed using a mechanical pipette with a 0.2 micron filter. This supernatant sample was then mixed with 5 milliliters of one molar nitric acid and stored for ICP-AES analysis of the total Sr, Mg, and Ca concentration. Any remaining solution in the aliquot was decanted. Ethanol was added to the centrifuge tube to return the total volume of the ACC sample to 25 mL before a second centrifugation for five minutes at the experimental temperature. The supernatant ethanol was then removed from the tube and the precipitate was allowed to air dry at ambient temperature under a fume hood. A subsample of the final solid material was dissolved in 1.0 molar nitric acid and stored for ICP-AES analysis. Reported values represent the average of three replicate experiments for each set of conditions. The experimental conditions used in this study are summarized in Table 3.

b. Transformation to crystalline products

The remaining ACC was stored in the incubator at the desired temperature without stirring and visually monitored until the ACC transformed. The transformation from ACC to calcite was complete when the colloidal suspension disappeared and a thin film of $CaCO_3$ formed at the bottom of the crystallization jar. Total time to transformation and the final pH of the system were recorded (Appendix A). The aliquot

extraction and centrifugation process was repeated for the crystalline solid samples and solution.

2. Synthesis of ACC Using a Flow-through Reactor

ACC was also synthesized using a flow-through reactor (Blue et al., in press). By mixing solutions at a fixed rate in a flowing system, this method brings the reaction solution to a constant "steady-state" chemistry that cannot be achieved by batch mixing. The composition of the solid precipitate is analyzed and compared to the measurements taken from the batch reaction.

The apparatus for these experiments consisted of a pump fitted with two 100 mL syringes. One syringe contained a reagent of $CaCl_2$ (SigmaAldrich, >99%), $MgCl_2$ (SigmaAldrich, >99%), and $SrCl_2$ (SigmaAldrich, 99%) at concentrations that gave the desired Mg/Ca ratio and Sr^{2+} concentration upon mixing (Table 3). The second syringe contained 100 mM sodium bicarbonate (SigmaAldrich, >99%) with pH adjusted to 9.5 using one molar NaOH. Both syringes were connected to opposite sides of a 26 mL reactor chamber. The solutions were then continuously pumped at 200 mL/hr into the reactor and mixed at 25°C. The solutions immediately precipitated ACC on contact. The suspended solid and solution exited the apparatus as an effluent via a part connected to polyethylene tubing at the top of the reactor.

The average residence time of solution in the reactor was two minutes. Collection of ACC occurred after a minimum of three residence times to allow the system to reach a steady state. Products were filtered through a 0.2 micron filter fitted over a vacuum flask. Each ACC sample was rinsed with ethanol and dried for 30 minutes before storing in a

vacuum desiccator. The samples were then weighed to determine the mass of ACC produced over the collection interval. A portion of the final ACC samples were dissolved in one molar nitric acid and stored for ICP-AES analysis. The experimental conditions used in this study are summarized in Table 3.

3. Analytical Methods

The compositions of solutions and solid precipitates were analyzed for total Ca, Mg, and Sr by inductively coupled plasma atomic emission spectroscopy (ICP-AES) using a Spectro ARCOS SOP. An yttrium internal standard was added to each sample in an internal standard mixing chamber (Glass Expansion, Inc.). Each sample then passed through a cross-flow nebulizer into a modified Scott-style spray chamber. The sample uptake rate was 2 milliliters per minute, with each sample analysis using 5 milliliters. The calibration standards for Ca, Mg, and Sr were from Environmental Express, Inc., and the second source check standards were from Spex, Inc..

The measurements of solution and solid precipitate compositions by ICP-AES were statistically analyzed using Microsoft Excel (Microsoft) and JMP Pro 10 (SAS). Best fit lines calculated by linear regression models weighed data points based on standard error. R^2 values were calculated to determine the correlation of data in the linear regression models. T-tests (Prob>|t|) were performed to determine the probability that the slope of a line was zero. The slope of a line is not statistically distinguishable from zero when the probability exceeds 5% (Prob>|t| $\geq$ 0.05).

The dry solid samples were analyzed by x-ray diffraction (XRD) using a Rigaku MiniFlex II to determine structure and crystallinity. Particles were placed on a silicon

zero-background mount to minimize background noise. Samples were analyzed with a copper source (K_α = 0.15418 nm) on a 2θ range between 20 and 70 with a step interval of 0.02 2θ and a dwelling time of five seconds per step.

The dry solid samples were imaged using a scanning electron microscope (SEM) with a FEI Quanta 600 FEG to determine particle size and morphology. Particles were placed on an SEM mount using an adherent carbon film. To prevent the sample from charging under the electron beam, the samples were sputter-coated with two nanometers of gold/palladium alloy. All samples were observed under an accelerating potential of 10 kV.

Results

1. Morphological Observations of ACC from Batch Synthesis

The morphology of the ACC products is shown in Figures 1 and 2. ACC is comprised of spherical particles that decrease in size with increased Mg content. This change in size is consistent with previous studies (Ajikumar et al., 2005; Wang et al., 2012). XRD analysis showed a single broadened hump across the 2θ range, consistent with the disorder of amorphous substances. ACC produced from the batch reactor experiments (Figures 1 and 2) may have undergone a small amount of re-precipitation, as evidenced by the cracked mosaic-like surface behind the ACC spheres. Exposure to open air and humidity after drying the solid product and transporting the sample may have resulted in dissolution and re-precipitation. This does not affect the composition measurements in any significant way, as the solids were immediately prepared for ICP-AES analysis after drying in ethanol.

The representative morphology of transformed crystalline products is shown in Figures 3 and 4. The surface morphology of the crystals consists of bladed to rhombohedral facets of $CaCO_3$. XRD analysis for the crystal products (Figure 5) shows shifts in the calcite 2θ peak positions of 0.5 at the 23.24, 29.6, 36.04, 39.62, 43.4, 47.7, and 48.66 peaks. The peaks are significantly broader than a calcite standard, most notably at the 47.7 and 48.66 2θ positions. Database analysis (ICDD) confirmed presence of high-Mg calcite for each experiment based on the 2θ shifts and peak broadening.

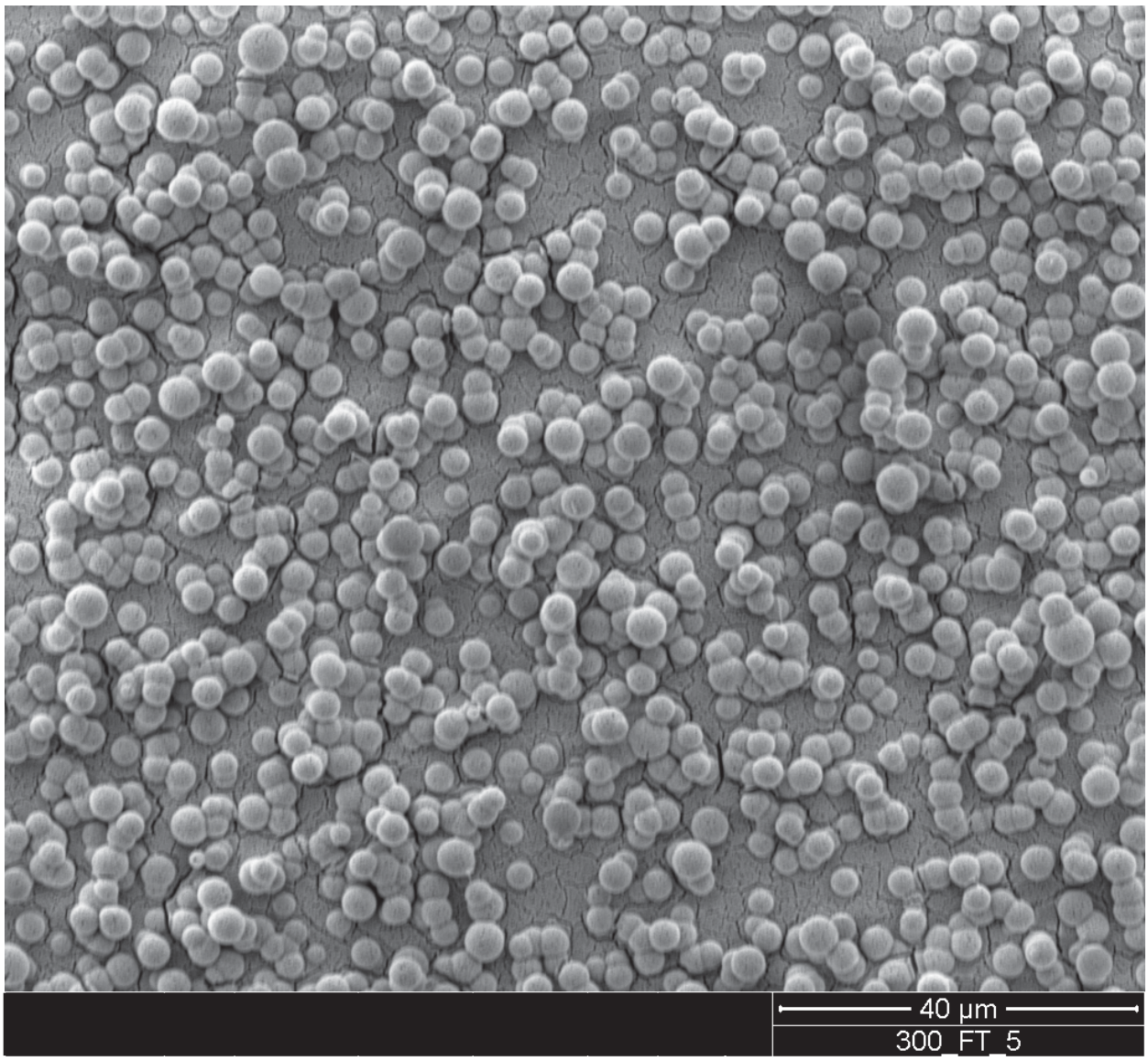

Figure 1: SEM image of ACC synthesized from 5/1 Mg/Ca and 1 mM Sr solution using the batch reaction method. The ACC morphology and sphere sizes are similar for all Mg and Sr concentrations.

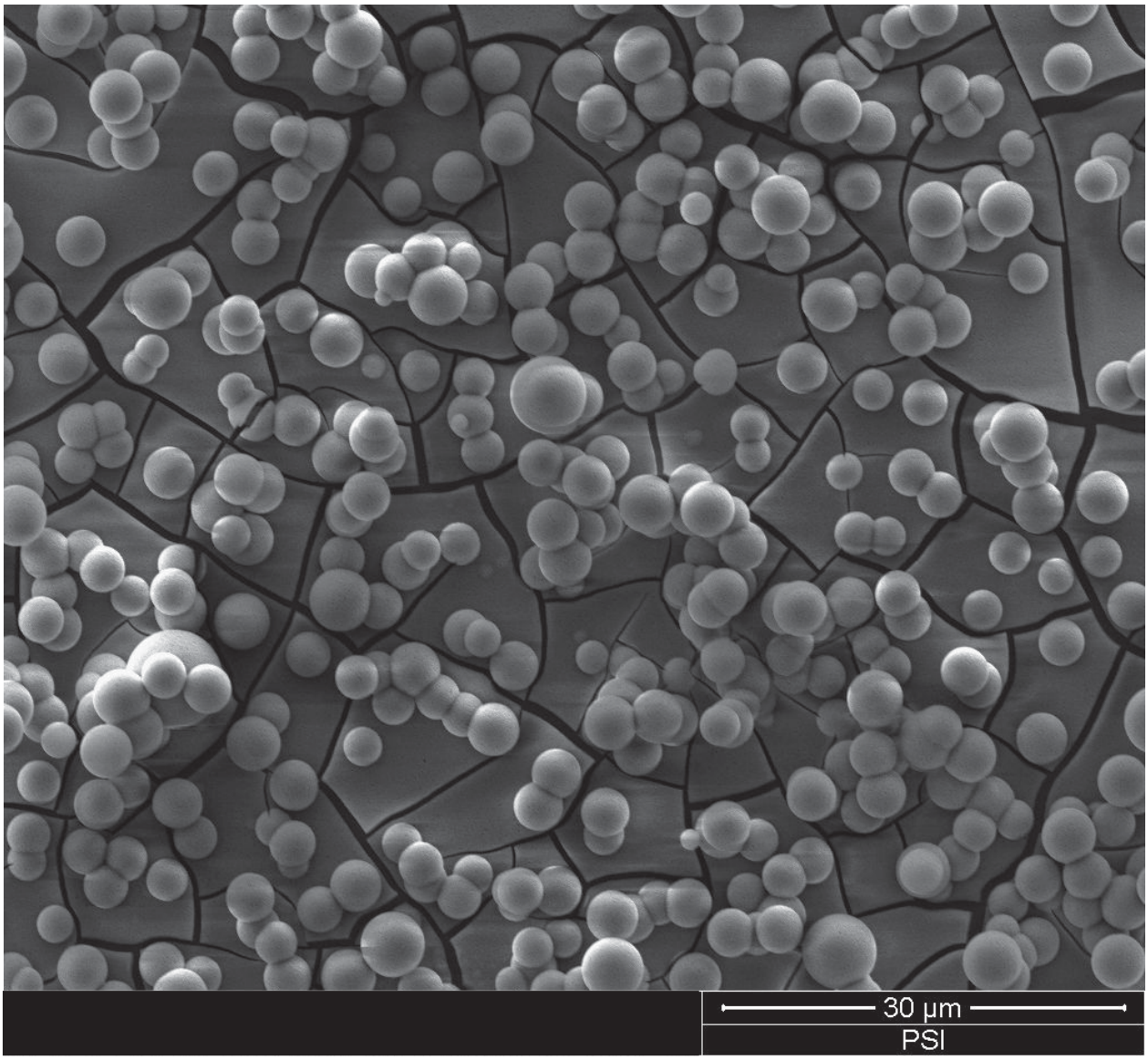

Figure 2: SEM image of ACC synthesized from 5/1 Mg/Ca and 1 mM Sr solution using the batch reaction method. The ACC morphology and sphere sizes are similar for all Mg and Sr concentrations.

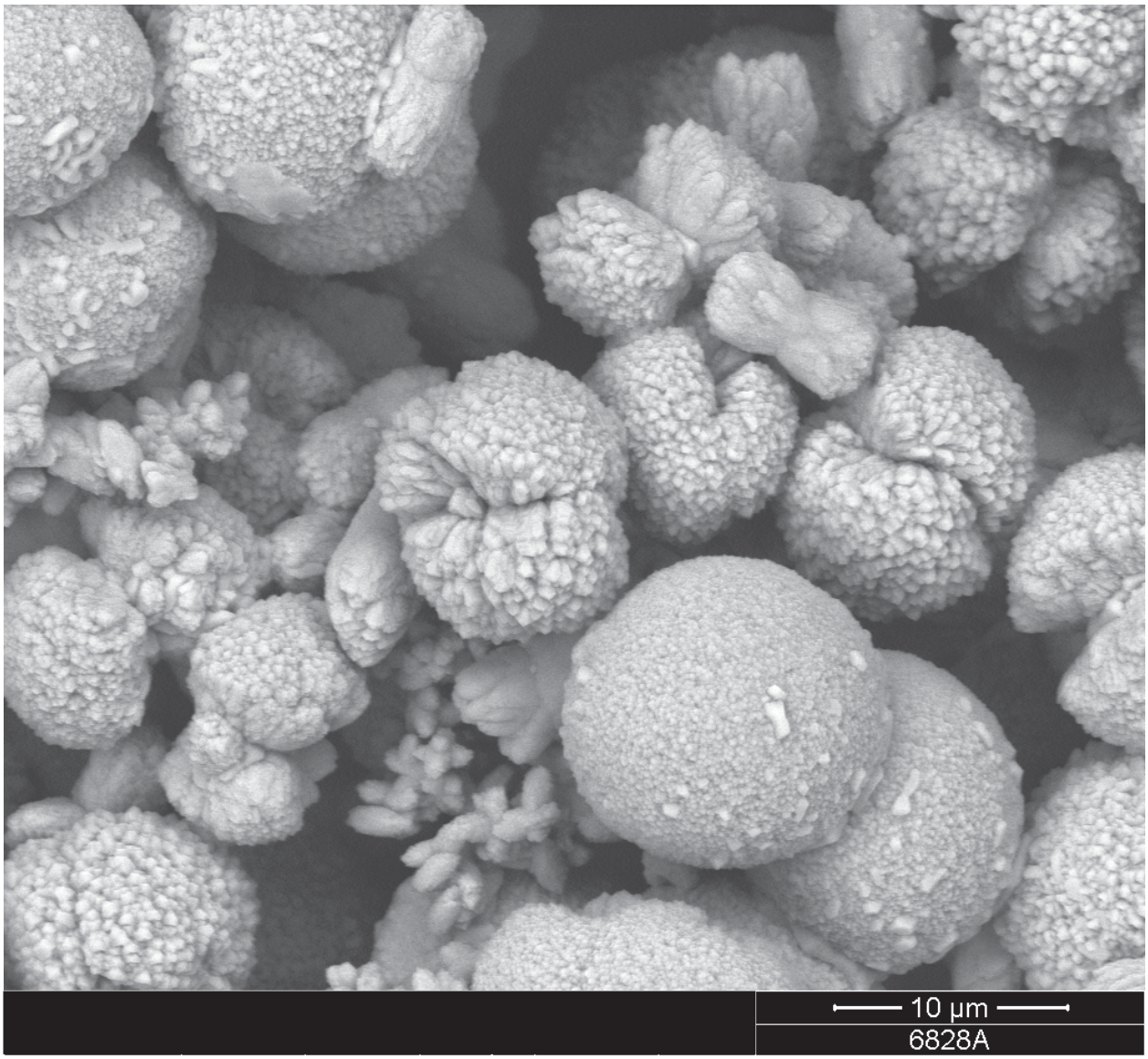

Figure 3: SEM image of high-Mg calcite that transformed from ACC. These products were synthesized from 5/1 Mg/Ca and 1 mM Sr solution at 25°C using the batch reaction method (see Table 2). The ACC morphologies are similar for all Mg and Sr concentrations.

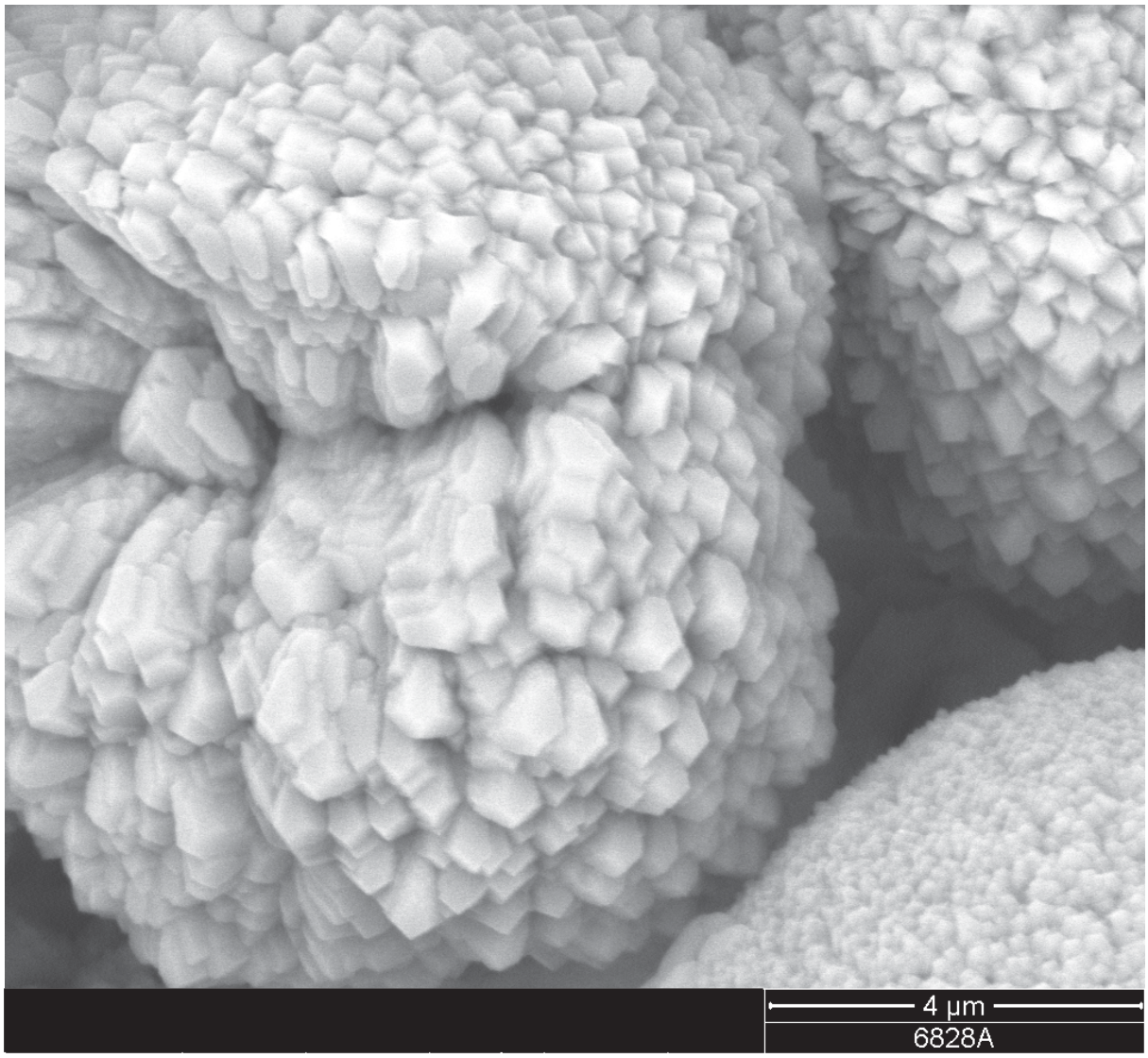

Figure 4: SEM image of high-Mg calcite that transformed from ACC. These products were synthesized from 5/1 Mg/Ca and 1 mM Sr solution at 25°C using the batch reaction method (see Table 2). The ACC morphologies are similar for all Mg and Sr concentrations.

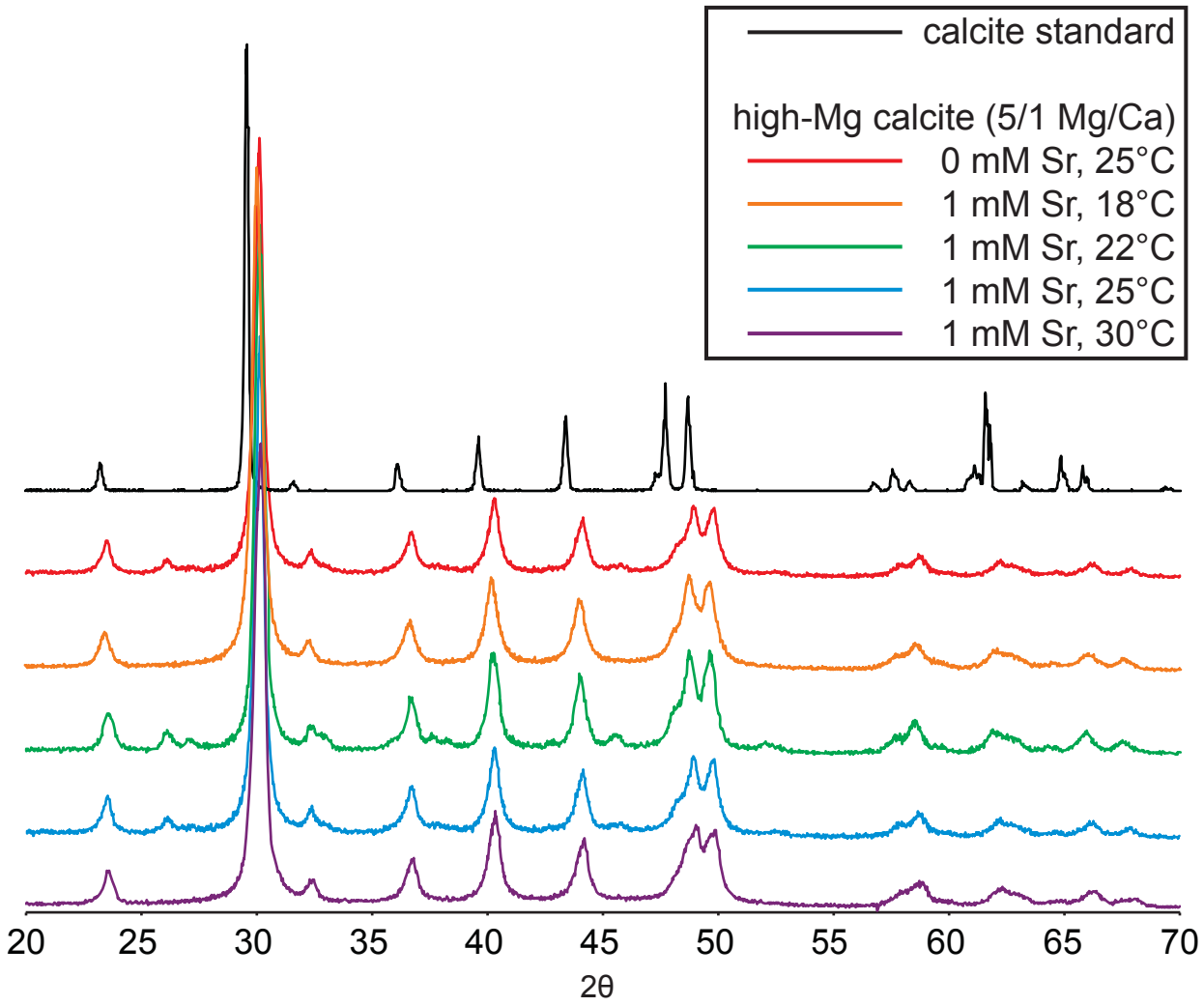

Figure 5: XRD spectra of batch reaction high-Mg calcites after ACC transformation, compared to a calcite standard. Peak broadening and lateral shift of the 2θ values for the 23.24, 29.6, 36.04, 39.62, 43.4, 47.7, and 48.66 peaks. The overall shift of 0.5 2θ indicates presence of Mg in the crystal lattice.

2. Composition Measurements

For each initial Sr concentration, Sr/Ca ratios in the ACC samples were analyzed with respect to Mg:Ca solution ratios to determine the effect of Mg on Sr uptake in batch reactor precipitation. The corresponding data in Figure 6 show that increases in Mg:Ca ratio suppresses Sr uptake in ACC by up to 25% at the highest initial Sr concentration of 1.0 mM Sr.

Cross-checking this result using the flow-through synthesis method shows a similar effect of Mg on Sr uptake in ACC. Increases in Mg:Ca ratio result in a decrease in Sr uptake in ACC up to a factor of 27% (Figure 7). After obtaining consistent solution and ACC composition data from both batch reactor and flow-through reactor methods, all further experiments were conducted via batch reactor. A summary of ICP-AES analyses of the precipitate and solution products is found in Appendix B.

3. Dependence of Composition on Temperature

The Sr/Ca ratio in ACC was determined across a range of temperatures and initial Sr concentrations to analyze the effect of temperature on Sr uptake. The data in Figure 8 show that temperature does not significantly affect Sr uptake into ACC, as seen by the subhorizontal trends of each data series, regardless of initial Sr. As expected, the measurements show offsets in the Sr/Ca composition of ACC as the initial Sr concentration increases, as shown by the labeled contours in Figure 8.

Upon transforming the ACC to high-Mg calcite, the Sr/Ca ratio of the solid product at each temperature was analyzed to determine the effect of temperature on the Sr content of the resultant crystalline phase. Figure 9 shows that temperature does not affect

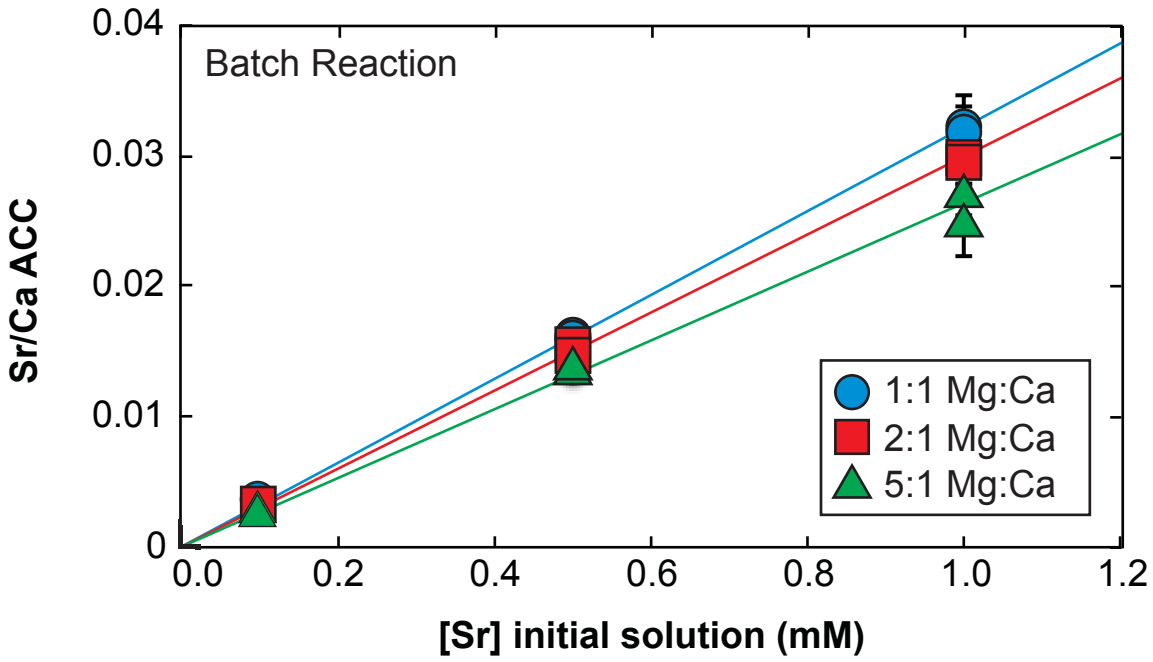

Figure 6: Sr/Ca ratios versus initial Sr concentration with respect to initial Mg/Ca ratios for batch reaction formation of ACC. The data are given in Appendix B, Table 1.

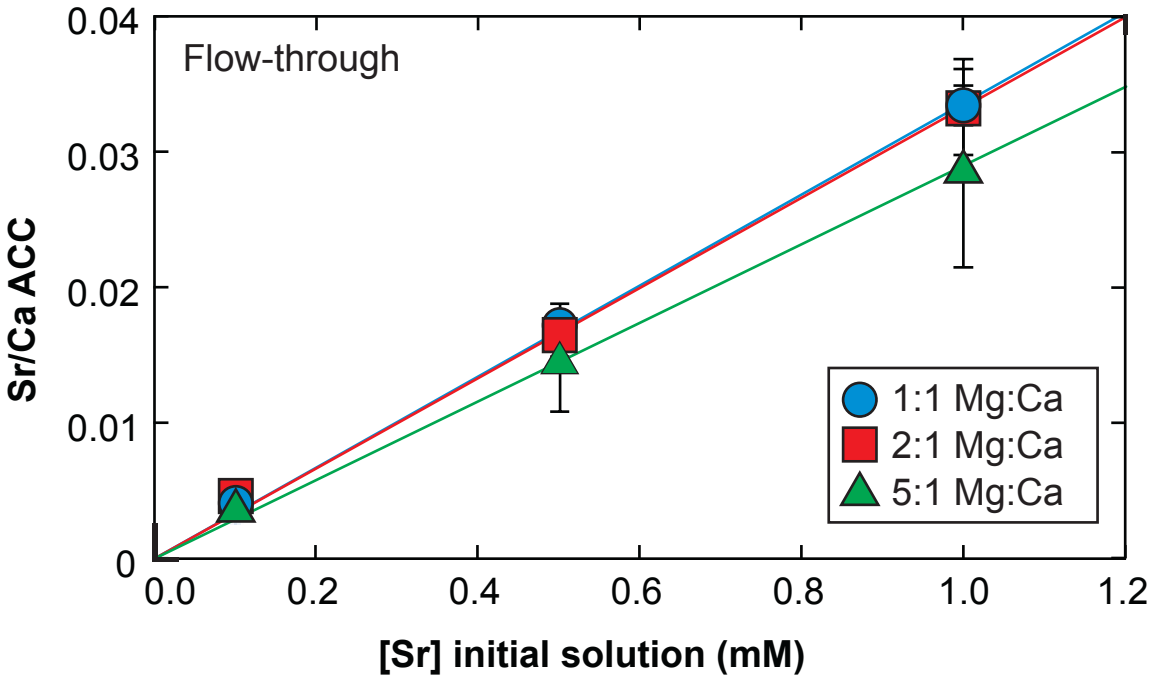

Figure 7: Sr/Ca ratios versus initial Sr concentration with respect to initial Mg/Ca ratios for flow-through reaction formation of ACC. The data are given in Appendix B, Table 2.

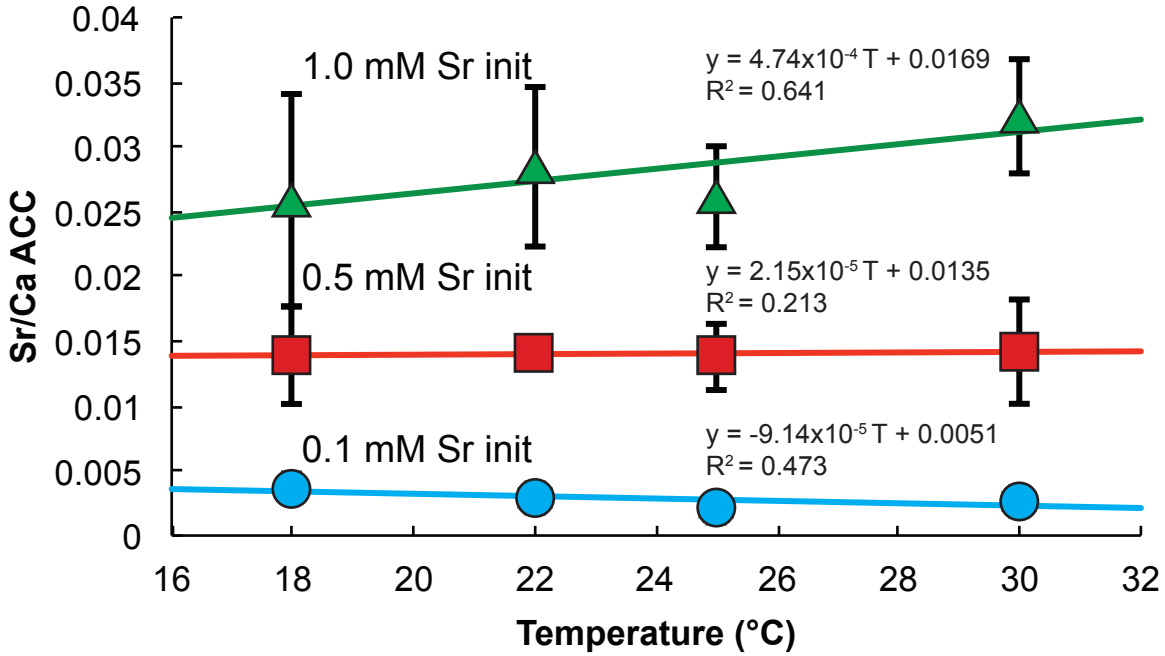

Figure 8: Sr/Ca of ACC versus temperature with respect to initial Sr concentration. The statistical probability of each slope being equal to zero (Prob>|t|) for the 0.1, 0.5, and 1.0 mM Sr concentrations are 0.4669, 0.2520, and 0.0963, respectively (SAS). Each symbol represents the mean of three individual experiments. The data are given in Appendix C, Tables 1 through 4.

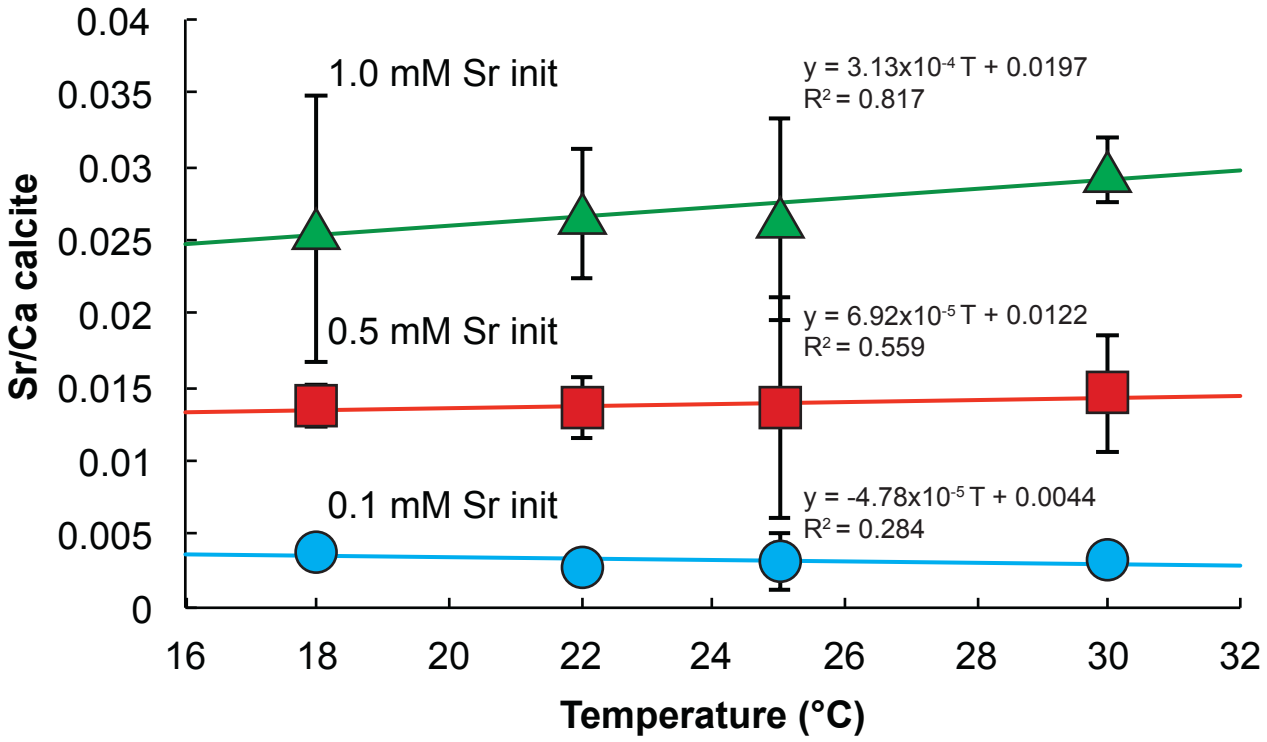

Figure 9: Sr/Ca of high-Mg calcite after ACC transformation versus temperature with respect to initial Sr concentration. The statistical probability of each slope being equal to zero (Prob>|t|) for the 0.1, 0.5, and 1.0 mM Sr concentrations are 0.4669, 0.2520, and 0.0963, respectively (SAS). Each symbol represents the mean of three individual experiments. The data are given in Appendix C, Tables 1 through 4.

the Sr composition of the resulting calcite. An increase in initial Sr concentration promotes Sr uptake in the resulting calcite as shown by the parallel contours of each data series. Combining the data in Figures 8 and 9 together for direct comparison, Figure 10 shows the Sr composition of the solid products does not significantly change after transformation.

The Mg/Ca ratio in ACC was also analyzed to determine the effect of temperature on Mg content. The data in Figure 11 shows the Mg/Ca ratio in ACC is independent of temperature for the 18-30°C range. The Mg/Ca of the resultant calcite was analyzed to determine the effect of temperature and transformation on the final product. In contrast, the trends in Figure 12 find a linear correlation between Mg/Ca in calcite and temperature with an increase of 0.004 Mg/Ca per °C ($y = 4.14 \cdot 10^{-3}\, T + 0.21$, R^2=0.647).

A summary of ICP-AES analyses of the solutions, ACC, and crystals is provided in Appendix C.

4. K_D and λ of Sr and Mg in Batch Reactor Experiments

To better understand the effect of Mg and temperature on the distribution of Sr into ACC and calcite, the distribution coefficients were calculated using Equation (3) to determine $K_{D,\,Sr}$ and $K_{D,\,Mg}$ in both the ACC and crystalline products of the temperature-controlled batch reactor experiments. The distribution coefficients of Sr in ACC show that $K_{D,\,Sr}$ is independent of synthesis temperature within standard error of the measurement (average $K_{D,\,Sr\,ACC}$ = 0.54±0.006) (Figure 13A, Table 1). The distribution coefficients of Sr in the high-Mg calcite produced by ACC transformation show that $K_{D,}$

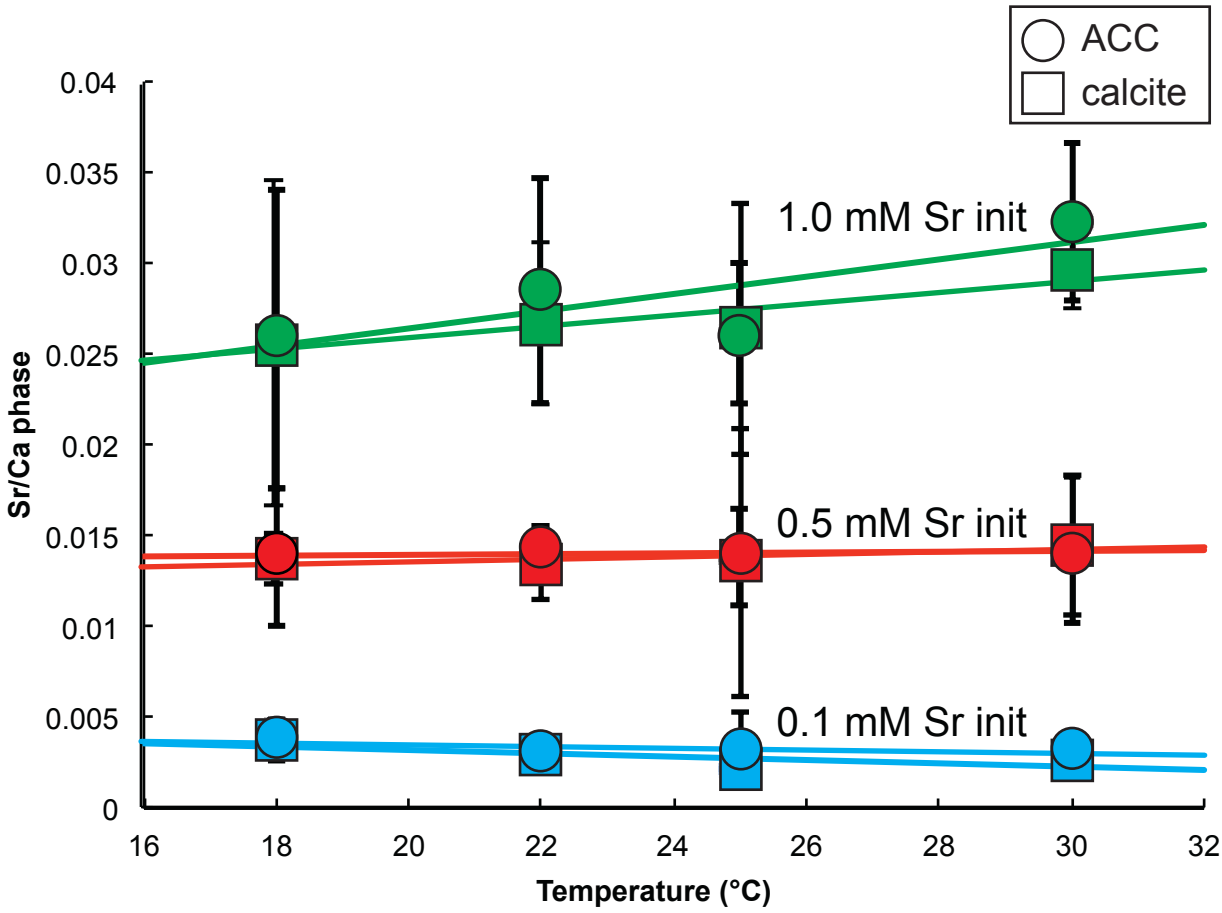

Figure 10: Overlay of Figures 8 and 9 show the Sr/Ca values of ACC and resultant calcite are not significantly different with respect to temperature and the initial Sr concentration.

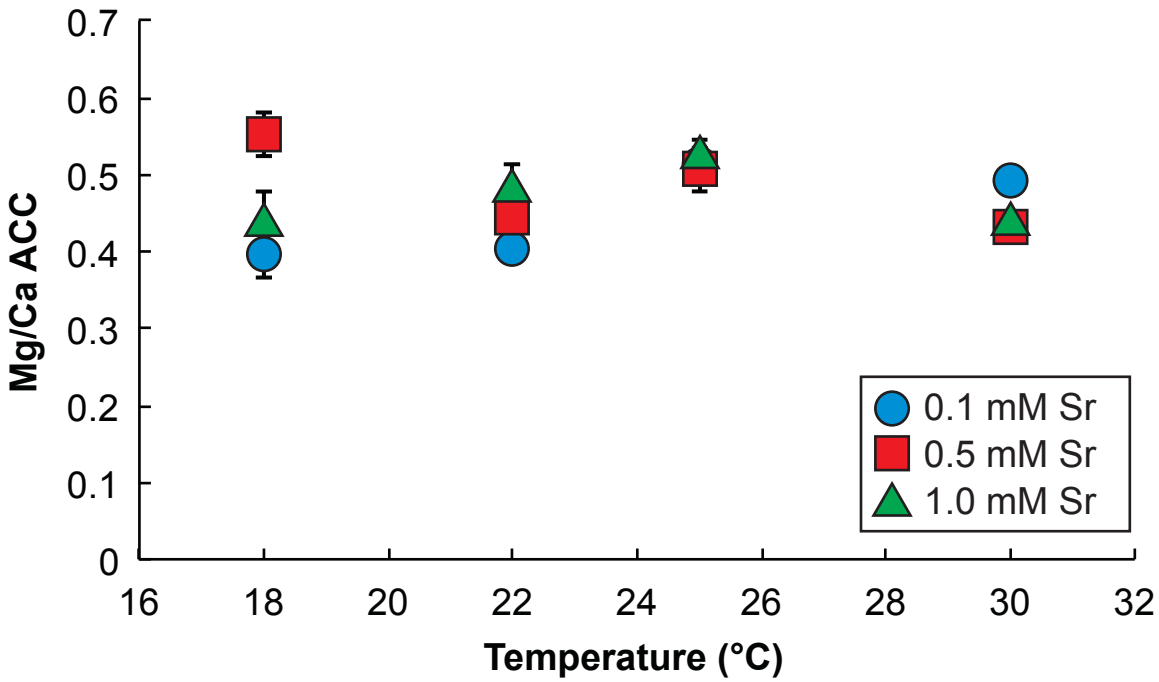

Figure 11: Mg/Ca of ACC versus temperature with respect to initial Sr concentrations. The data are given in Appendix C, Tables 1 through 4.

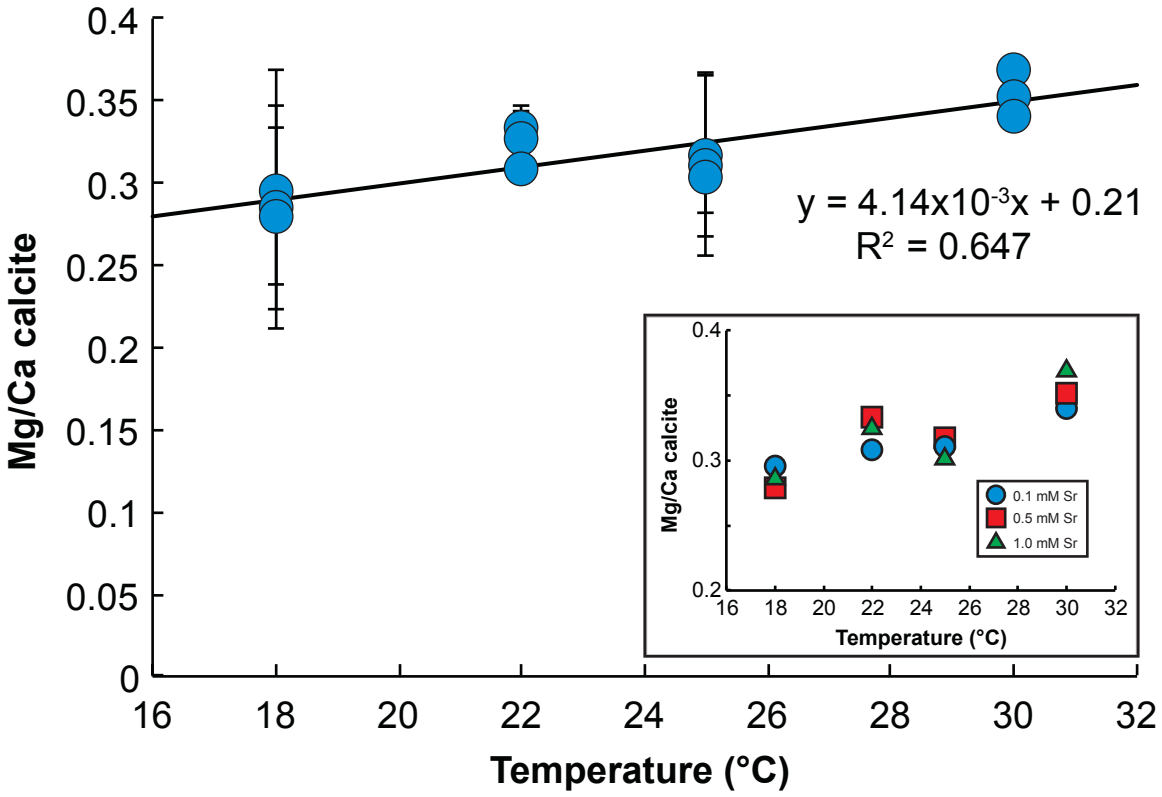

Figure 12: Mg/Ca of high-Mg calcite after ACC transformation versus temperature with respect to initial Sr concentration. Data used in the linear regression is weighted based on standard error. The data are given in Appendix C, Tables 1 through 4.

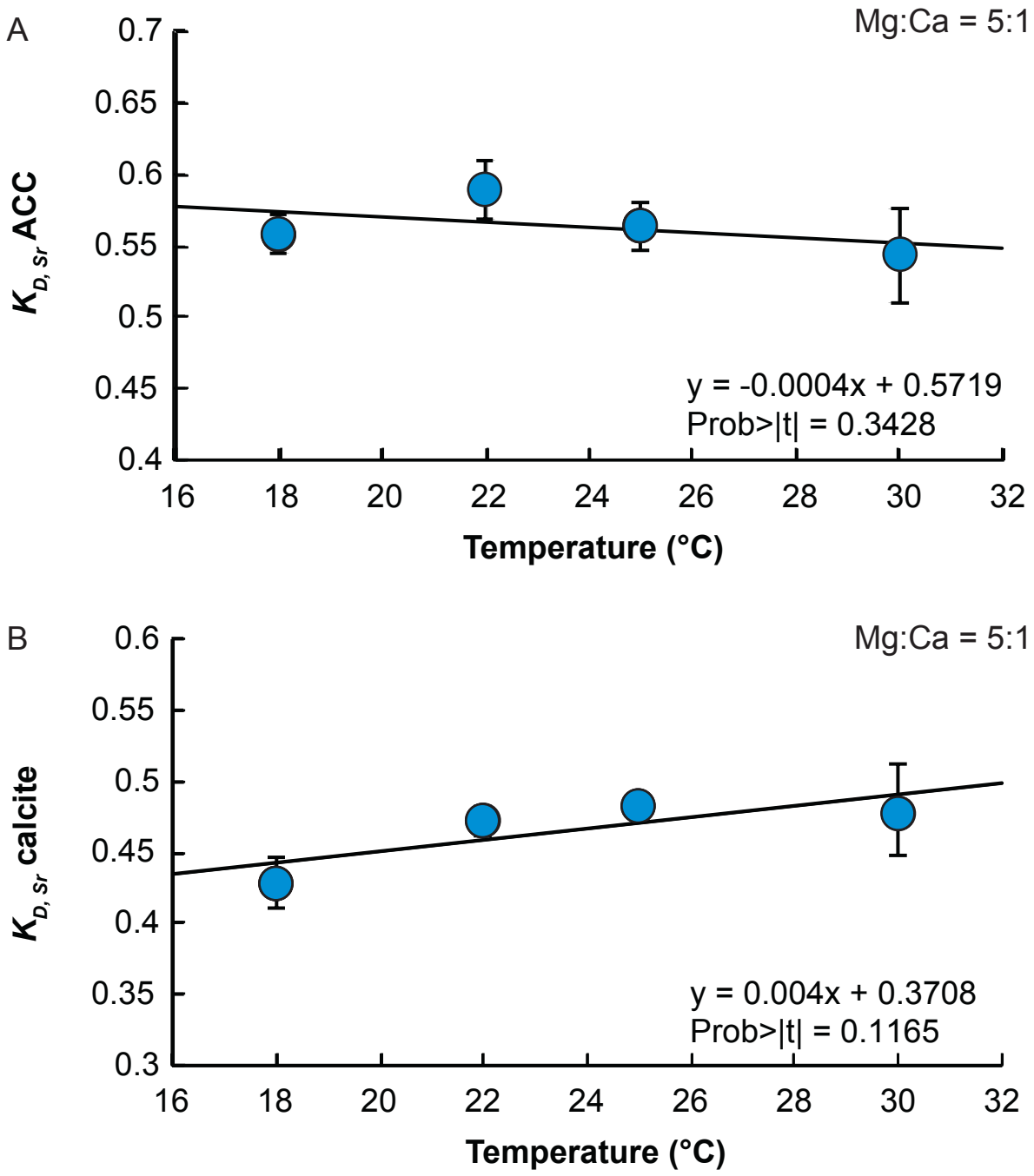

Figure 13: Distribution coefficients of Sr in batch reactor (A) ACC (Figure 8) and (B) resultant high-Mg calcite (Figure 9) with respect to temperature. Statistical analysis of all values obtained across experiments shows that $K_{D, Sr\ ACC} = 0.543 \pm 0.006$ and $K_{D, Sr\ calcite} = 0.466 \pm 0.009$ (Table 1). Data used in the linear regression is weighted based on standard error of the mean ($s/\sqrt{n}$). The t-tests show that the slopes of the lines are not statistically distinguishable from zero.

$_{Sr}$ is independent of temperature (average $K_{D,\ Sr\ calcite}$ = 0.47±0.005) (Figure 13B, Table 1). $K_{D,Sr}$ values calculated from each experiment are shown in Table 4.

The λ_{Sr} values in both the ACC and crystalline products of the temperature-controlled batch reactor experiments were calculated using Equation (4). The partition coefficients of Sr in ACC show that λ_{Sr} is independent of synthesis temperature within standard error of the measurement (average $\lambda_{Sr\ ACC}$ = 0.66±0.006) (Figure 14A, Table 1). The partition coefficients of Sr in the high-Mg calcite produced by ACC transformation show that λ_{Sr} is independent of temperature (average $\lambda_{Sr\ calcite}$ = 0.60±0.008) (Figure 14B, Table 1). λ_{Sr} values calculated from each experiment are shown in Table 5.

The distribution coefficients of Mg in ACC show a subhorizontal linear correlation of $K_{D,\ Mg}$ across temperature (average $K_{D,\ Mg,\ ACC}$ = 0.056±0.0009) (Figure 15A, Table 2). The distribution coefficients of Mg in the high-Mg calcite produced by ACC transformation show a similar subhorizontal trend (average $K_{D,\ Mg,\ calcite}$ = 0.023±0.0004) (Figure 15B, Table 2). $K_{D,\ Mg}$ values calculated from each experiment are shown in Table 4.

The λ_{Mg} values in ACC show a subhorizontal linear correlation across temperature (average $\lambda_{Mg,\ ACC}$ = 0.017±0.0012) (Figure 16A, Table 2). The distribution coefficients of Mg in the high-Mg calcite produced by ACC transformation show a similar subhorizontal trend (average $\lambda_{Mg,\ calcite}$ = 0.094±0.0011) (Figure 16B, Table 2). λ_{Mg} values calculated from each experiment are shown in Table 5.

Table 4: Experimental conditions and distribution coefficients obtained for ACC and calcite produced by the batch reactor and flow-through reactor (MFR) methods. Each experiment was conducted using initial 25 mM $CaCl_2$ and 125 mM $MgCl_2$ solutions (Mg/Ca = 5/1).

		ACC						Calcite	
		Mg/Ca = 1/1		Mg/Ca = 2/1		Mg/Ca = 5/1		Mg/Ca = 5/1	
T (°C)	[Sr] (mM)	$K_{D, Mg}$	$K_{D, Sr}$	$K_{D, Mg}$	$K_{D, Sr}$	$K_{D, Mg}$	$K_{D, Sr}$	$K_{D, Mg}$	$K_{D, Sr}$
18	0.1					0.048	0.575	0.018	0.464
18	0.5					0.053	0.568	0.017	0.419
18	1.0					0.054	0.532	0.020	0.404
22	0.1					0.052	0.622	0.021	0.477
22	0.5					0.047	0.552	0.026	0.453
22	1.0					0.049	0.595	0.030	0.489
25	0.1 (batch)	0.071	0.774	0.066	0.689	0.073	0.584	0.026	0.484
25	0.1 (MFR)	0.026	0.463	0.020	0.239	0.098	0.788		
25	0.5 (batch)	0.063	0.626	0.058	0.657	0.053	0.576	0.029	0.488
25	0.5 (MFR)	0.013	0.882	0.014	0.909	0.095	0.937		
25	1.0 (batch)	0.055	0.573	0.054	0.649	0.058	0.530	0.030	0.475
25	1.0 (MFR)	0.043	1.071	0.055	0.987	0.195	0.806		
30	0.1					0.062	0.591	0.014	0.547
30	0.5					0.068	0.561	0.022	0.452
30	1.0					0.060	0.479	0.027	0.440

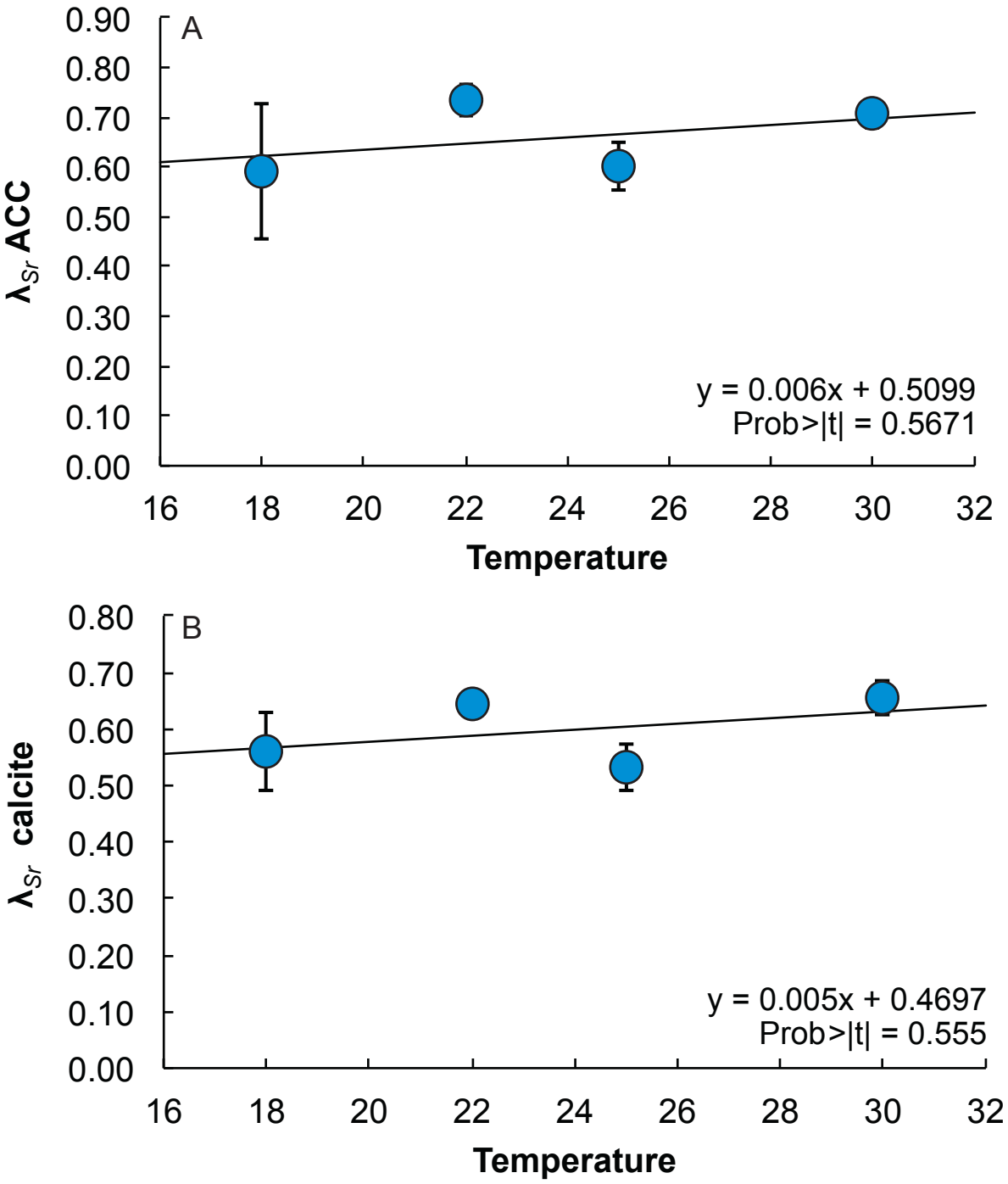

Figure 14: Distribution coefficients (λ) of Sr in batch reactor (A) ACC (Figure 8) and (B) resultant high-Mg calcite (Figure 9) with respect to temperature. Statistical analysis of all values obtained across experiments shows that $\lambda_{Sr\ ACC} = 0.66 \pm 0.006$ and $\lambda_{Sr\ calcite} = 0.60 \pm 0.008$. Data used in the linear regression is weighted based on standard error of the mean ($s/\sqrt{n}$). The t-tests show that the slopes of the lines are not statistically distinguishable from zero.

Table 5: Conditions and Doerner-Hoskins distribution coefficients for temperature-varied batch reactor experiments. Each experiment was conducted with 25 mM $CaCl_2$ and 125 mM $MgCl_2$ (Mg/Ca = 5/1). All *m* values reported in mM.

ACC

T (°C)	m_{Sr}^{o}	m_{Mg}^{o}	m_{Ca}^{o}	m_{Sr}	m_{Mg}	m_{Ca}	λ_{Sr}	λ_{Mg}
18	0.1	125	25	0.08	115.28	11.99	0.32	0.11
18	0.5	125	25	0.29	106.11	11.87	0.73	0.22
18	1.0	125	25	0.59	108.15	12.05	0.72	0.20
22	0.1	125	25	0.06	111.88	13.19	0.80	0.17
22	0.5	125	25	0.28	105.55	10.63	0.69	0.20
22	1.0	125	25	0.58	112.98	11.66	0.71	0.13
25	0.1	125	25	0.07	106.56	12.08	0.52	0.22
25	0.5	125	25	0.31	109.99	12.43	0.68	0.18
25	1.0	125	25	0.69	121.69	13.61	0.60	0.04
30	0.1	125	25	0.07	104.56	14.96	0.73	0.35
30	0.5	125	25	0.32	104.30	12.59	0.65	0.26
30	1.0	125	25	0.43	97.19	8.19	0.76	0.23

Calcite

T (°C)	m_{Sr}^{o}	m_{Mg}^{o}	m_{Ca}^{o}	m_{Sr}	m_{Mg}	m_{Ca}	λ_{Sr}	λ_{Mg}
18	0.1	125	25	0.06	116.8	6.91	0.42	0.05
18	0.5	125	25	0.20	102.3	6.06	0.65	0.14
18	1.0	125	25	0.49	113.5	7.76	0.60	0.08
22	0.1	125	25	0.05	110.0	7.65	0.67	0.11
22	0.5	125	25	0.26	111.2	8.78	0.62	0.11
22	1.0	125	25	0.57	115.7	10.46	0.64	0.09
25	0.1	125	25	0.07	119.3	10.00	0.45	0.05
25	0.5	125	25	0.31	119.8	11.02	0.60	0.05
25	1.0	125	25	0.68	123.9	12.12	0.54	0.01
30	0.1	125	25	0.04	107.6	7.18	0.71	0.12
30	0.5	125	25	0.24	105.7	7.46	0.61	0.14
30	1.0	125	25	0.38	97.0	5.70	0.65	0.17

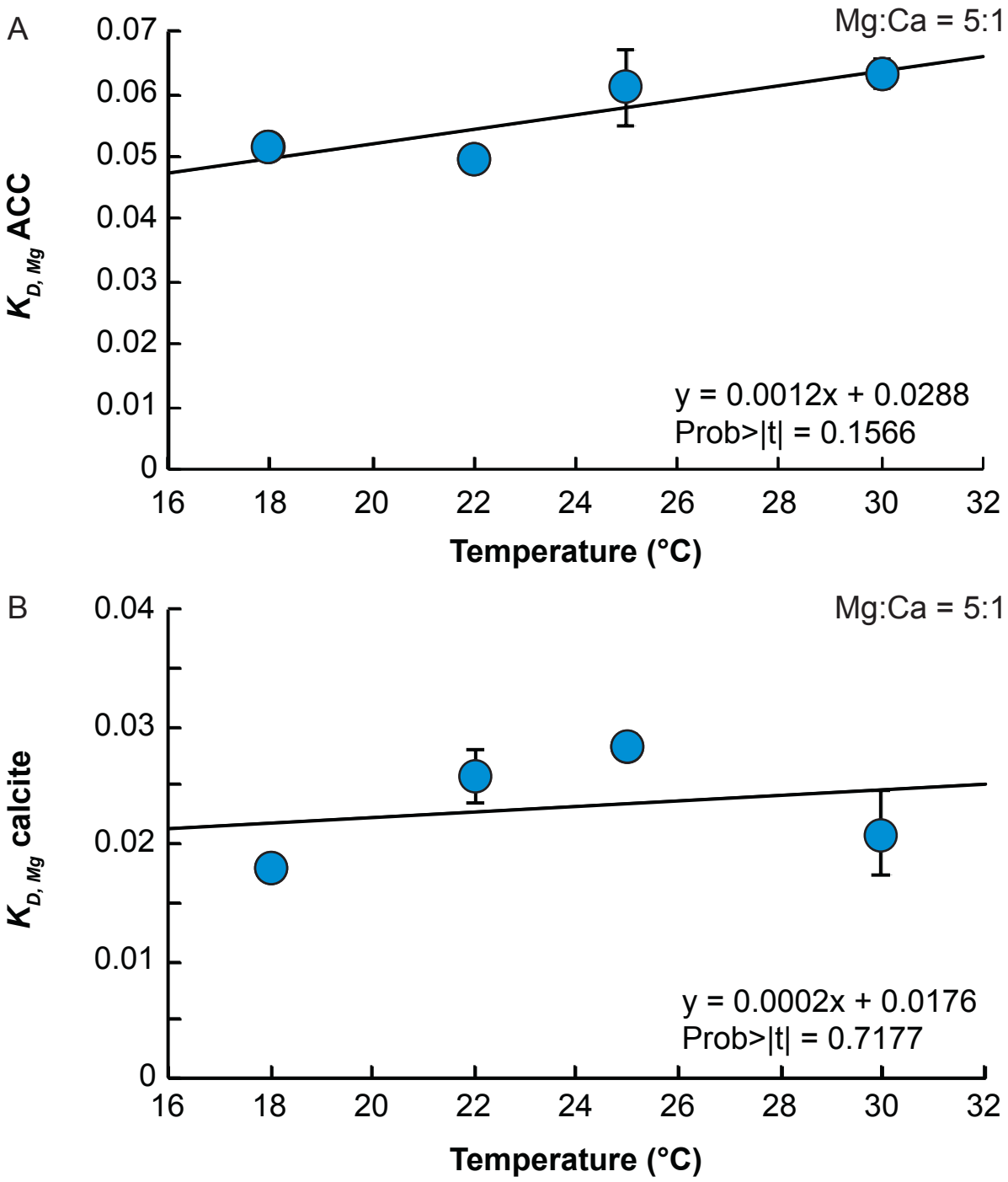

Figure 15: Distribution coefficients of Mg in batch reactor (A) ACC (Figure 8) and (B) resultant high-Mg calcite (Figure 9) with respect to temperature. Statistical analysis of all values obtained across experiments shows that $K_{D,Mg\ ACC} = 0.0564 \pm 0.0009$ and $K_{D,Mg\ calcite} = 0.0232 \pm 0.0004$. Data used in the linear regression is weighted based on standard error of the mean ($s/\sqrt{n}$). The t-tests show that the slopes of the lines are not statistically distinguishable from zero.

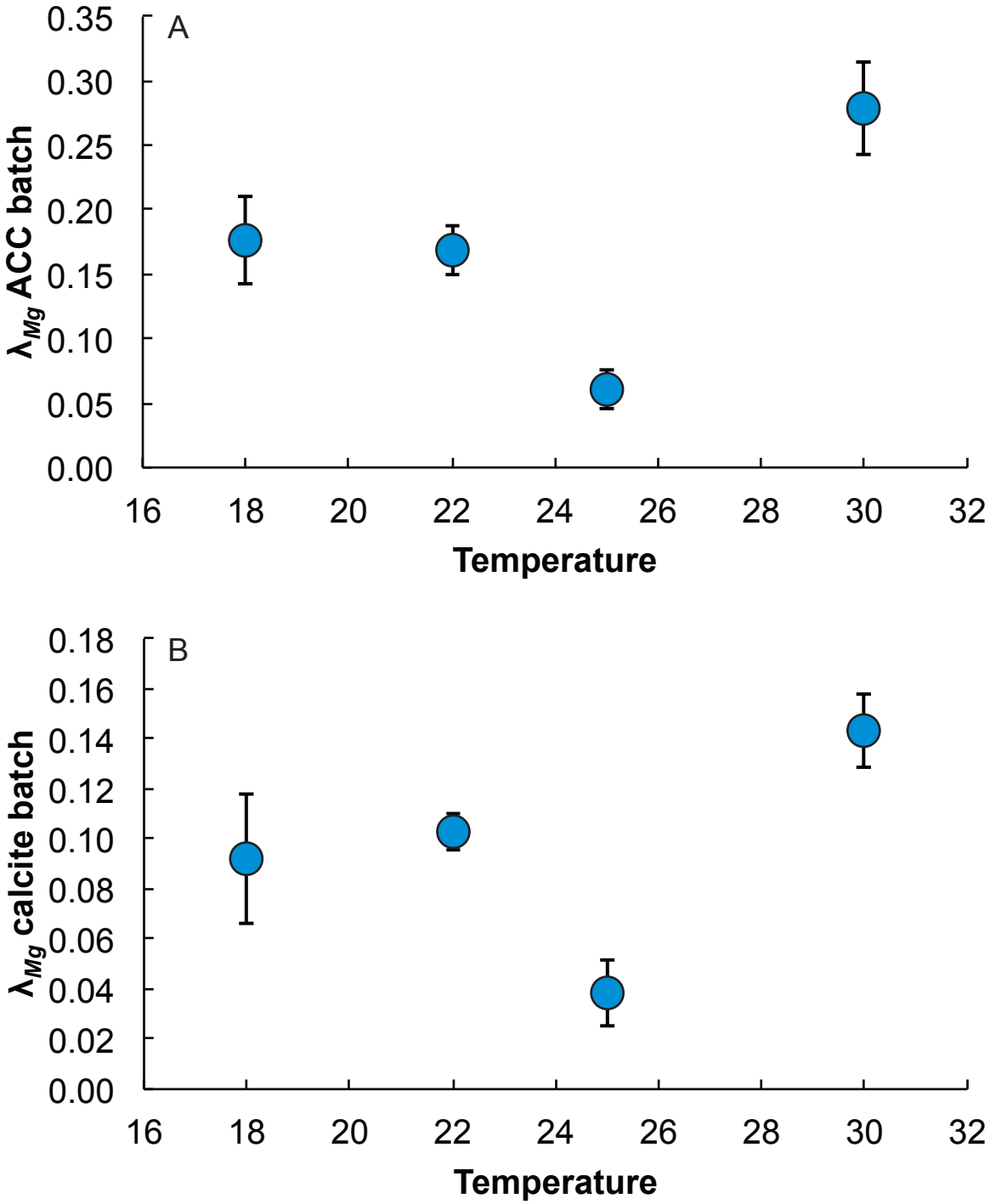

Figure 16: Distribution coefficients (λ) of Mg in batch reactor (A) ACC (Figure 8) and (B) resultant high-Mg calcite (Figure 9) with respect to temperature. Statistical analysis of all values obtained across experiments shows that $\lambda_{Mg\ ACC} = 0.017 \pm 0.0012$ and $\lambda_{Mg\ calcite} = 0.094 \pm 0.0011$. Data used in the linear regression is weighted based on standard error of the mean ($s/\sqrt{n}$).

5. K_D of Sr and Mg in Flow-Through Reactor Experiments

To compare the effects of the two methods used to precipitate ACC, the distribution coefficients were calculated using Equation (3) to determine $K_{D,\,Sr}$ and $K_{D,\,Mg}$ in the ACC products of the flow-through reactor experiments (Tables 1 and 2). The distribution coefficients of Sr in ACC display varying trends with respect to increased Mg/Ca ratio (Figure 17A). $K_{D,\,Sr}$ values in flow-through reactor ACC show an increase in distribution coefficient with respect to initial Sr concentration at Mg/Ca ratios of 1/1 and 2/1, and the $K_{D,\,Sr}$ values at a Mg/Ca ratio of 5/1 show no dependence on initial Sr (Figure 18). The distribution coefficients of Mg in ACC show an increase of $K_{D,\,Mg}$ with respect to Mg/Ca (Figure 17B).

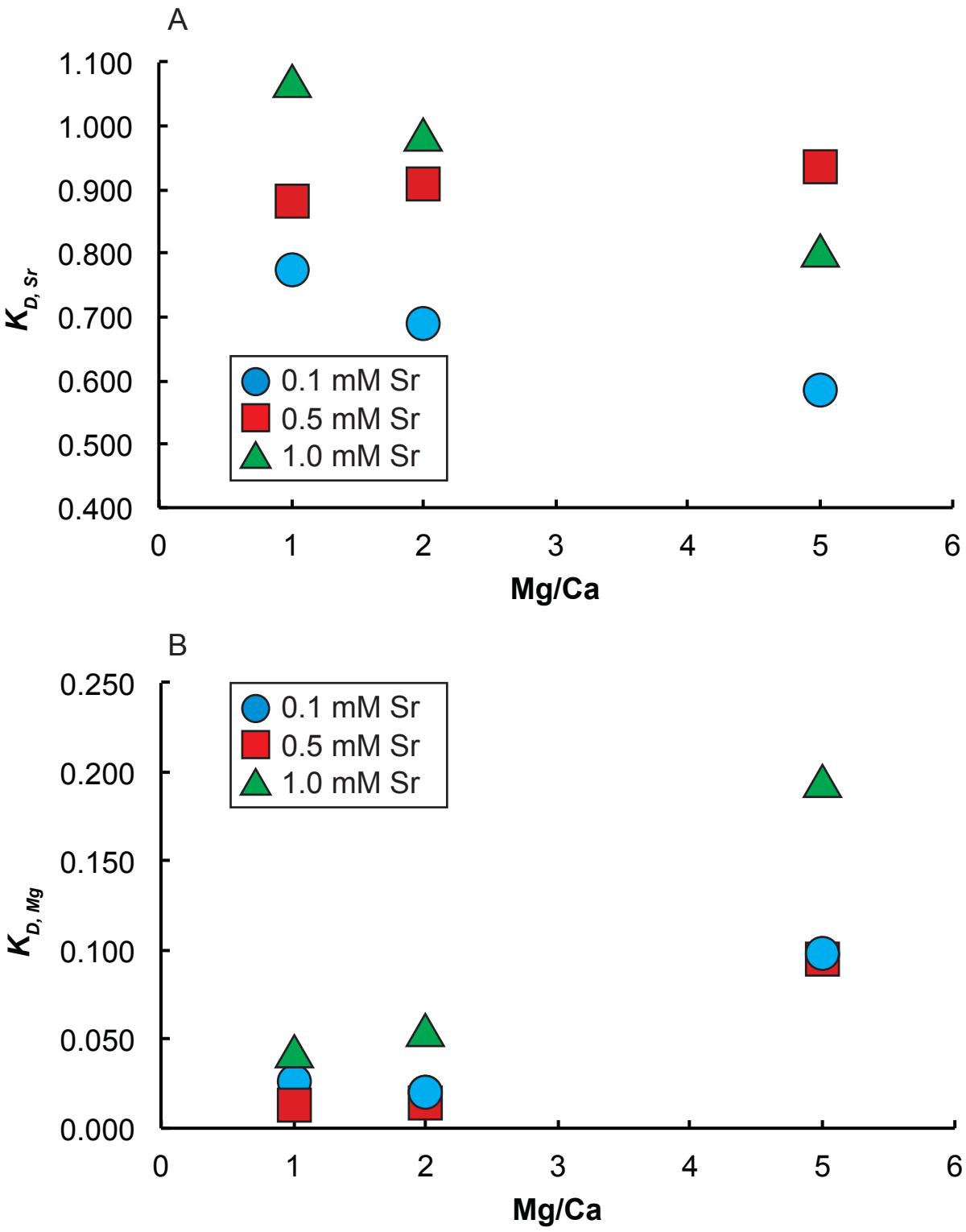

Figure 17: Distribution coefficients of (A) Sr and (B) Mg in flow-through reactor ACC with respect to Mg/Ca ratio. The data are given in Table 3.

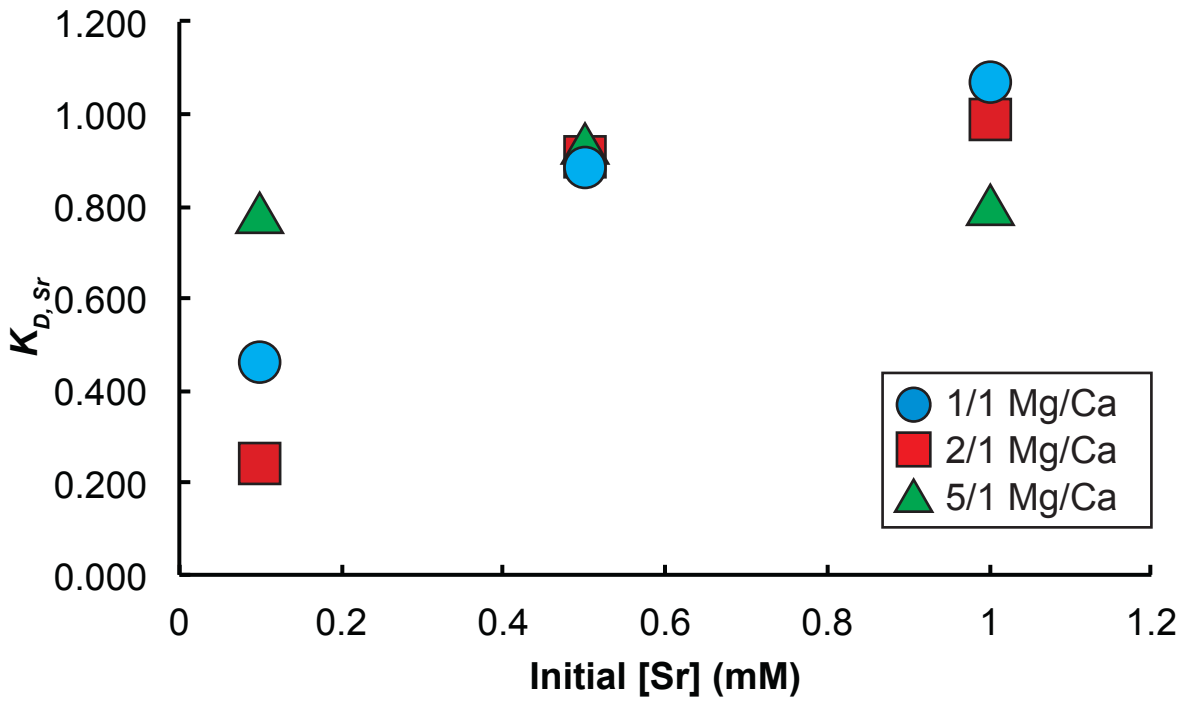

Figure 18: Distribution coefficients of Sr in flow-through reactor ACC with respect to initial Sr concentration. The data are given in Table 3.

Discussion

1. Experimental Observations

The batch reactor temperature experiments were conducted at a Mg:Ca ratio of 5:1 to reflect natural seawater cation ratios used in previous laboratory experiments (Mucci and Morse, 1983) and culturing studies of marine calcifiers (Lorens and Bender, 1980). The cation concentrations used in the batch reactor and flow-through experiments are 150% higher than natural seawater concentrations. Previous studies show that higher concentrations of Mg in solution increase ACC stability and slow the rate of transformation to calcite over long periods of time (Meldrum and Colfen, 2008; Wang, 2009; Han et al., data unpublished). The concentrations used in this study may have impacted the transformation time (Appendix A) and composition of the ACC during transformation.

2. ACC

a. Sr Uptake is Suppressed by Mg in ACC

The findings show that increases in Mg suppress Sr uptake into ACC in both the batch reactor and flow-through reactor (Figure 6). ACC precipitated in the 5:1 Mg:Ca solution contains 25% less Sr than ACC in the 1:1 Mg:Ca solution. Both Mg and Sr substitute for Ca in the calcite crystal lattice and form a solid solution (Paquette and Reeder, 1990; Pingitore et al., 1992). In the classical crystal growth model, presence of the smaller Mg^{2+} and larger Sr^{2+} ions result in disordered calcite structures as a function of preferential kink site binding for each ion (Paquette and Reeder, 1995). While the kinetics of ACC formation are unknown, the hydration spheres of the cations may affect

the nucleation of the metastable phase and the uptake of other cations with different hydration energies (Wang et al., 2009).

b. Sr/Ca in ACC is Independent of Temperature

The Sr/Ca ratio of the batch reactor ACC is independent of temperature for the 18-30°C range (Figure 8). This relationship contrasts with inorganic classical crystal growth experiments that show an increase in Sr/Ca ratio in calcite with respect to increase in temperature (Malone and Baker, 1999). It is possible that increasing the range of temperatures will yield a dependence of Sr/Ca on temperature, although this exceeds natural seawater conditions relevant to biogenic mineralization.

c. K_D and λ for Sr and Mg in ACC are Independent of Temperature

The $K_{D,\,Sr}$ and λ_{Sr} values of ACC do not change with respect to temperature (Figures 13A and 14A). This contrasts with investigations of crystalline $CaCO_3$ where increases in temperature resulted in higher $K_{D,\,Sr}$ values (Katz, 1972; Malone and Baker, 1999). The distribution of other trace elements in ACC may be similar to Sr, as seen in classical growth experiments (Curti, 1999), although no such study has been conducted for ACC. The $K_{D,\,Mg}$ values of ACC are independent of temperature (Figure 15A) and are consistent with distribution coefficients found in previous investigations (Sawada et al., 1990; Blue et al., in press). The Mg distribution coefficients for ACC are also consistent with values found in step-growth inorganic calcite (Winland, 1969).

d. $K_{D,\,Sr}$ for ACC is Significantly Higher than $K_{D,\,Sr}$ for Classical and Biogenic Calcite

The distribution coefficients of the batch reactor ACC are greater than the $K_{D,\,Sr}$ values of inorganic calcites by an order of magnitude (Tables 1 and 3). Similarly, the $K_{D,\,Sr}$ values of ACC obtained in this study exceed those found in biogenic calcites by up to a factor of four. While the distribution coefficients of ACC alone do not fully account for the composition of the resultant calcite, the higher $K_{D,\,Sr}$ suggests that calcite formation by the ACC pathway can localize up to ten times more concentrations of Sr in ACC prior to crystal transformation. It is plausible that the Sr ions are more readily incorporated into an amorphous structure that forms without the restrictions of step-growth kinetics, thereby resulting in the high $K_{D,\,Sr}$ value for ACC (Paquette and Reeder, 1995).

The estimates of $K_{D,\,Sr}$ and $K_{D,\,Mg}$ for ACC reported in Tables 1 and 3 and Figures 13A and 14A are based on the assumption that Sr rapidly equilibrates throughout the solid by diffusion within the time of ACC precipitation in the batch reactor. It is possible that the cores of ACC particles contain lower amounts of Sr and Mg because the Sr/Ca and Mg/Ca ratios of the solutions increase over the duration of each experiment, producing a gradient of increasing Sr and Mg concentration from the core to the outer edge of the particle. The Sr/Ca and Mg/Ca ratios of the solution after the two separate ACC extractions after mixing are similar, however, suggesting that complete precipitation of ACC occurs within two minutes of mixing.

e. $K_{D,\,Sr}$ and $K_{D,\,Mg}$ Values for ACC in the Batch Reactor and Flow-Through Reactor Methods Contrast

The distribution coefficients of the flow-through reactor ACC are different from the $K_{D,\,Sr}$ values of the batch reactor ACC for each Mg/Ca ratio and initial Sr concentration (Figure 17A and Table 3). This discrepancy raises the question of which method is best for precipitating ACC in a steady state environment. The data in Figures 6 and 7 show that Sr/Ca values for ACC are similar for both experimental methods. This suggests that the discrepancy in $K_{D,\,Sr}$ values pertains to the Sr/Ca ratio of the steady state solution. The volume of ACC produced in the flow-through reactor may have resulted in precipitate build-up in the reactor chamber, increasing the residence time of ACC in the reactor and changing the solution chemistry. It is also possible that the filter paper used in the flow-through reactor experiments absorbed some of the effluent solution during collection, altering the concentration of the sampled solution and the resulting $K_{D,\,Sr}$ and $K_{D,\,Mg}$ values.

The distribution coefficients of Mg in the flow-through reactor increase with the initial Mg/Ca ratio (Figure 17B). This data contrasts with the finding that $K_{D,\,Mg}$ in batch reactor ACC is independent of Mg/Ca (Table 3). It is possible that the higher residence time of the batch reactor generated a more consistent steady state than the flow-through reactor, resulting in a constant $K_{D,\,Mg}$ value.

The finding that Sr distribution coefficients in ACC precipitated at low Mg/Ca ratios in the flow-through reactor experiments is dependent on initial Sr concentration contrasts with the findings that ACC precipitated in the batch reactor is independent of temperature (Figure 18 and Table 3). This trend is not seen at the 5/1 Mg/Ca ratio,

suggesting that an increase of Mg/Ca may decrease the dependence of $K_{D, Sr}$ on Sr concentration in the flow-through reactor. It is possible that the lower residence time of the flow-through reactor relative to that of the batch reactor results in a better measurement of Sr/Ca ratios near the time the reaction takes place, while the higher residence time of the batch reactor method results in more consistent values after the reaction reaches steady state.

f. K_D and λ Values for Sr and Mg in ACC Contrast

The $K_{D, Sr}$ and $K_{D, Mg}$ values of the batch reactor ACC are different from the λ_{Sr} and λ_{Mg} values of the batch reactor ACC (Table 2). This discrepancy calls into question which calculation is better suited for the precipitation reaction. Table 2 shows that for each batch reactor experiment, the Mg/Ca and Sr/Ca ratios of the solutions increases as ACC precipitates. It is possible that as the ACC particles form and grow, a gradation of increasing Mg and Sr from the center occurs, resulting in a different K_D value than otherwise predicted by the Doerner-Hoskins model.

3. Resultant Calcite

a. Sr/Ca in Resultant Calcite is Independent of Temperature

The Sr/Ca ratio of the high-Mg calcite that formed via ACC in the batch reactor experiments is independent of temperature on the 18-30°C range (Figure 9). Temperature also does not affect the morphology of the resultant batch-reactor calcite (Figure 5). The findings contrast with studies of classically grown calcite that report a temperature dependence (Malone and Baker, 1999). This apparent discrepancy between this study and

biogenic calcite measurements may explain why Sr is not a reliable proxy for temperature across a wide range of calcifying species (Rosenthal et al., 1997; Wanamaker et al., 2008). It is plausible that any temperature dependence shown in the Sr/Ca of organically precipitated calcite is an apparent trend caused by different vital effects (Lea, 1999). The finding that Sr/Ca in ACC and calcite is independent of temperature calls into question the usage of Sr/Ca in biogenic calcites as a paleotemperature proxy without understanding the physical basis for the apparent trends that are reported in the literature.

b. Sr/Ca Ratios from ACC Transformation to Resultant Calcite Do Not Change

For each initial Sr concentration and temperature, the Sr/Ca ratios of the batch reactor ACC and resultant high-Mg calcite are similar (Figure 10). The composition of the crystalline product is established with the formation of ACC. It was hypothesized that the phase transformation itself would result in a lower Sr/Ca ratio in calcite during the redistribution of ions from an amorphous state to the calcite structure. Because the $K_{D,\,Sr}$ value of ACC is higher than the $K_{D,\,Sr}$ value of the resultant calcite, it is possible that Sr and Ca are excluded from the ACC in equal proportions during transformation due to a decrease in phase solubility, resulting in a constant Sr/Ca ratio from amorphous to crystalline phase.

c. K_D and λ Values for Sr and Mg in Calcite are Independent of Temperature

The $K_{D,\,Sr}$ and λ_{Sr} values of the resultant calcite are independent of temperature (Figure 13B and 14B). This contrasts with investigations of classically grown calcites where increases in temperature resulted in higher $K_{D,\,Sr}$ (Katz, 1972; Malone and Baker,

1999). While the temperature range of this study is relevant to biogenic calcites, a larger temperature range may reveal a temperature dependence of Sr distribution coefficients for high-Mg calcite. The distribution of Sr in calcite formed via ACC may be similar for other trace elements similar to Sr, although no such study has been conducted. $K_{D,\,Mg}$ values in the resultant calcite are also independent of temperature. This relationship is consistent with trends found in step-growth inorganic calcite (Winland, 1969).

d. $K_{D,\,Sr}$ of Calcite Formed via ACC is Significantly Higher than $K_{D,\,Sr}$ for Classical and Biogenic Calcite

The Sr distribution coefficients of calcite that formed from ACC exceed the values reported by classical experiments by a factor of four (Table 1). The higher $K_{D,Sr}$ values suggest that the mineralization pathway affects Sr distribution in calcite. The high $K_{D,Sr}$ values reported for ACC may directly affect the $K_{D,Sr}$ value for the resultant calcite. During transformation, the Sr may leave the solid phase altogether, resulting in a $K_{D,\,Sr}$ value for calcite that is lower than that for ACC. Alternatively, the Sr may remain in the solid phase and incorporate into the calcite crystal, producing a $K_{D,\,Sr}$ value higher than those reported in by classical calcite growth experiments.

The $K_{D,\,Sr}$ values obtained for the transformed calcite exceed the values reported by biogenic calcite studies by a factor of three (Table 1). This difference raises the question of whether the organisms listed in Table 1 may utilize the non-classical ACC to calcite mineralization pathway. If the organisms do precipitate calcite via an ACC intermediate phase, it is possible that other vital effects affect the trace element composition of the biogenic calcite.

The findings of Paquette and Reeder (1995) emphasize the notion that empirical distribution coefficients are a function of availability of ion incorporation sites, which can vary with crystal surface structure and external growth conditions. The amorphous setting has no structural restrictions, which may allow Sr to more readily enter ACC. The crystalline setting is controlled by the periodic structure of calcite and the formation of kink sites and step edges on the growth surface. The Sr atom is larger than the Ca atom, and thus does not easily fit into the calcite crystal, as supported by low K_D values in calcites grown by the classical process (see Table 1). The limited attachments in kink-step growth decrease as impurities such as Sr attach to available sites (Wasylenki, 2005; de Yoreo, 2009). The differences between an amorphous versus crystalline environment contribute to the larger $K_{D,\,Sr}$ values reported for the resultant calcite and may explain the lower $K_{D,\,Sr}$ values for experiments that utilized classical calcite growth or transformation to a crystal seed (Holland, 1964; Kitano, 1971).

Conclusions

This study raises several questions regarding trace element distribution in calcifying organisms. The finding that Sr/Ca ratios of calcite formed by a non-classical mineralization pathway are independent of temperature contrasts with measurements from biogenic calcite studies that show a temperature dependence. It is possible that other "vital effects", such as the influence of organic macromolecules, are cause for the apparent discrepancy between biogenic calcite Sr/Ca ratios and the inorganic calcite Sr/Ca ratios quantified in this study. A previous study shows macromolecules affects the Mg content of ACC (Wang et al., 2009), and a similar effect may influence the uptake of Sr and other trace elements in both ACC and the resultant calcite. Careful analysis of the biomineralization processes and environments for individual calcifying species may resolve the differences in temperature dependence trends.

The finding that Sr/Ca ratios remain constant after the transition from ACC to calcite has implications for understanding the physical basis of the non-classical mineralization pathway. It has been shown in ACC transformation experiments that Sr isotopes incorporate from the solution to the solid phase during the transition to crystalline $CaCO_3$ (Giuffre, in prep.), suggesting dissolution during transformation. The introduction of impurities to a steady state aqueous environment that contains ACC may influence the transformation or trace element uptake of the amorphous and crystalline phases.

The significantly higher values of $K_{D,\,Sr}$ and λ_{Sr} for both ACC and calcite that are measured in this study compared to values reported for biogenic Sr distribution coefficients are intriguing. This discrepancy raises the question of whether $K_{D,\,Sr}$ and λ_{Sr}

values could be used as an indicator of mineralogical pathway used by a particular organism, in whole or in part. To my knowledge, measurements of trace element distribution coefficients for the calcitic biominerals of modern species that utilize ACC have not been conducted. It would be interesting for future live culturing or field studies that focus on trace element incorporation to determine $K_{D,Sr}$ and λ_{Sr} in tandem with the type of mineralization process that is used by the organism during biomineralization.

The different measurements for element distribution coefficients in the batch reactor and flow-through reactor methods, in addition to the differences between this study and the measurements of previous work, raises the question of which type of experimental method is better for understanding elemental signatures in calcite. These discrepancies reiterate the limitations of this type of approach to understanding the concepts of K_D and λ, as well as the factors that influence element incorporation during mineralization.

The experiments conducted in this study did not vary saturation state, salinity, and pH, but such a study would provide further insight into the effects of chemical driving force, ionic strength, and ion speciation on the non-classical mineralization process. As our understanding of past environmental conditions is refined, and as our predictions of future conditions improve, the mechanisms of trace element incorporation in minerals that have formed over geologic time can be studied with greater precision.

References:

Addadi, L., Raz, S., & Weiner, S. (2003). "Taking advantage of disorder: amorphous calcium carbonate and its roles in biomineralization". Advanced Materials **15**(12), 959-970.

Ajikumar, P. K., Wong, L. G., Subramanyam, G., Lakshminarayanan, R., & Valiyaveettil, S. (2005). "Synthesis and characterization of monodispersed spheres of amorphous calcium carbonate and calcite spherules." Crystal Growth & Design, **5**(3): 1129-1134.

Bender, M. L., Lorens, R. B., & Williams, D. F. (1975). "Sodium, magnesium and strontium in the tests of planktonic foraminifera". Micropaleontology 448-459.

Beniash, E., Aizenberg, J., Addadi, L., & Weiner, S. (1997). "Amorphous calcium carbonate transforms into calcite during sea urchin larval spicule growth." Proceedings of the Royal Society of London. Series B: Biological Sciences **264**(1380): 461-465.

Blue, C.R., & Dove, P.M. (2013). "Chemical controls on the Magnesium content of Amorphous Calcium Carbonate". In press, Geochimica et Cosmochimica Acta.

Cohen, A. L., Layne, G. D., Hart, S. R., & Lobel, P. S. (2001). "Kinetic control of skeletal Sr/Ca in a symbiotic coral: Implications for the paleotemperature proxy." Paleoceanography **16**(1): 20-26.

Cölfen, H., & Antonietti, M. (2005). "Mesocrystals: inorganic superstructures made by highly parallel crystallization and controlled alignment". Angewandte Chemie International Edition **44**(35), 5576-5591.

Curti, E. (1999). "Coprecipitation of radionuclides with calcite: estimation of partition coefficients based on a review of laboratory investigations and geochemical data". Applied Geochemistry **14**(4): 433-445.

de Nooijer, L. J., Toyofuku, T., & Kitazato, H. (2009). "Foraminifera promote calcification by elevating their intracellular pH". Proceedings of the National Academy of Sciences **106**(36): 15374-15378.

de Yoreo, J. J., Zepeda-Ruiz, L. A., Friddle, R. W., Qiu, S. R., Wasylenki, L. E., Chernov, A. A., Gilmer, G.H., & Dove, P. M. (2009). "Rethinking classical crystal growth models through molecular scale insights: consequences of kink-limited kinetics". Crystal Growth & Design **9**(12): 5135-5144.

Dissard, D., Nehrke, G., Reichart, G. J., & Bijma, J. (2010). "Impact of seawater pCO2 on calcification and Mg/Ca and Sr/Ca ratios in benthic foraminifera calcite: results from culturing experiments with *Ammonia tepida*." Biogeosciences **7**: 81.

Doerner, H. A., & Hoskins, W. M. (1925). "CO-PRECIPITATION OF RADIUM AND BARIUM SULFATES". Journal of the American Chemical Society **47**(3): 662-675.

Elderfield, H., Bertram, C. J., & Erez, J. (1996). "A biomineralization model for the incorporation of trace elements into foraminiferal calcium carbonate." Earth and Planetary Science Letters **142**(3): 409-423.

Epstein, S., Buchsbaum, R., Lowenstam, H., & Urey, H. C. (1951). "Carbonate-water isotopic temperature scale". Geological Society of America Bulletin **62**(4): 417-426.

Epstein, S., & Mayeda, T. (1953). "Variation of O^{18} content of waters from natural sources". Geochimica et Cosmochimica Acta **4**(5): 213-224.

Freitas, P., Clarke, L. J., Kennedy, H., Richardson, C., & Abrantes, F. (2005). "Mg/Ca, Sr/Ca, and stable‐isotope (δ18O and δ13C) ratio profiles from the fan mussel *Pinna nobilis*: Seasonal records and temperature relationships". Geochemistry, Geophysics, Geosystems **6**(4).

Gebauer, D., Völkel, A., & Cölfen, H. (2008). "Stable prenucleation calcium carbonate clusters." Science **322**(5909): 1819-1822.

Giuffre et al. (2013). In prep.

Glover, E. D., Sippel, R. F. (1967). "Synthesis of magnesium calcites." Geochimica et Cosmochimica Acta **31**: 603-613.

Han, N. & Dove, P.M. (2013). Data unpublished.

Hiebenthal, C. (2009). "Sensitivity of A. islandica and M. edulis towards environmental changes: a threat to the bivalves; an opportunity for palaeo-climatology?". Doctoral dissertation, Kiel, Christian-Albrechts-Universität.

Holland, H. D., Holland, H. J., & Munoz, J. L. (1964). "The coprecipitation of cations with CaCO< sub> 3</sub>—II. The coprecipitation of Sr^{2+} with calcite between 90° and 100° C". Geochimica et Cosmochimica Acta **28**(8): 1287-1301.

Jacob, D. E., Soldati, A. L., Wirth, R., Huth, J., Wehrmeister, U., & Hofmeister, W. (2008). "Nanostructure, composition and mechanisms of bivalve shell growth." Geochimica et Cosmochimica Acta **72**(22), 5401-5415.

Katz, A. M. I. T. A. I., Sass, E., Starinsky, A., & Holland, H. D. (1972). "Strontium behavior in the aragonite-calcite transformation: An experimental study at 40–98 C". Geochimica et Cosmochimica Acta **36**(4): 481-496.

Kitano, Y., Kanamori, N., & Oomori, T. (1971). "Measurements of distribution coefficients of strontium and barium between carbonate precipitate and solution–

Abnormally high values of distribution coefficients measured at early stages of carbonate formation". Geochemical Journal **4**: 183-206.

Kossel, W. (1927). "Zur Theorie des Kristallwachstums". Nachrichten von der Gesellschaft der Wissenschaften zu Göttingen. Mathematisch-Physikalische Klasse: 135-143.

Lea, D.W., Mashiotta, T.A., Spero, H.J. (1999). "Controls on magnesium and strontium uptake in planktonic foraminifera determined by live culturing." Geochimica et Cosmochimica Acta **63**: 2369–2379

Lorens, R. B. (1981). "Sr, Cd, Mn and Co distribution coefficients in calcite as a function of calcite precipitation rate". Geochimica et Cosmochimica Acta **45**(4): 553-561.

Lorens, R. B., & Bender, M. L. (1980). "The impact of solution chemistry on *Mytilus edulis* calcite and aragonite". Geochimica et Cosmochimica Acta **44**(9): 1265-1278.

Lorrain, A., Gillikin, D. P., Paulet, Y. M., Chauvaud, L., Le Mercier, A., Navez, J., & André, L. (2005). "Strong kinetic effects on Sr/Ca ratios in the calcitic bivalve *Pecten maximus*". Geology **33**(12): 965-968.

Malone, M. J., & Baker, P. A. (1999). "Temperature dependence of the strontium distribution coefficient in calcite: An experimental study from 40 to 200 C and application to natural diagenetic calcites". Journal of Sedimentary Research **69**(1).

Meldrum, F. C., & Colfen, H. (2008). "Controlling Mineral Morphologies and Structures in Biological and Synthetic Systems". Chemical Reviews **108**: 4332-4432.

Mucci, A., & Morse, J. W. (1983). "The incorporation of Mg^{2+} and Sr^{2+} into calcite overgrowths: influences of growth rate and solution composition." Geochimica et Cosmochimica Acta **47**(2), 217-233.

Oomori, T., Kaneshima, H., Maezato, Y., & Kitano, Y. (1987). "Distribution coefficient of Mg^{2+} ions between calcite and solution at 10–50°C". Marine Chemistry **20(**4): 327-336.

Paquette, J., & Reeder, R. J. (1990). "New type of compositional zoning in calcite: Insights into crystal-growth mechanisms". Geology **18**(12): 1244-1247.

Paquette, J., & Reeder, R. J. (1995). "Relationship between surface structure, growth mechanism, and trace element incorporation in calcite". Geochimica et Cosmochimica Acta **59**(4): 735-749.

Pingitore, N. E., & Eastman, M. P. (1986). "The coprecipitation of Sr^{2+} with calcite at 25° C and 1 atm." Geochimica et Cosmochimica Acta **50(**10): 2195-2203.

Pingitore, N. E., Lytle, F. W., Davies, B. M., Eastman, M. P., Eller, P. G., Larson, E. M. (1992). "Mode of incorporation of Sr^{2+} in calcite: Determination by X-ray absorption spectroscopy." Geochimica et Cosmochimica Acta **56**(4): 1531-1538.

Radha, A. V., Forbes, T. Z., Killian, C. E., Gilbert, P. U. P. A., & Navrotsky, A. (2010). "Transformation and crystallization energetics of synthetic and biogenic amorphous calcium carbonate". Proceedings of the National Academy of Sciences **107**(38): 16438-16443.

Rosenthal, Y., Boyle, E. A., & Slowey, N. (1997). "Temperature control on the incorporation of magnesium, strontium, fluorine, and cadmium into benthic foraminiferal shells from Little Bahama Bank: Prospects for thermocline paleoceanography". Geochimica et Cosmochimica Acta **61**(17): 3633-3643.

Russell, A. D., Hönisch, B., Spero, H. J., & Lea, D. W. (2004). "Effects of seawater carbonate ion concentration and temperature on shell U, Mg, and Sr in cultured planktonic foraminifera." Geochimica et Cosmochimica Acta **68**(21): 4347-4361.

Sand, K. K., Rodriguez-Blanco, J. D., Makovicky, E., Benning, L. G., & Stipp, S. L. S. (2012). "Crystallization of $CaCO_3$ in Water−Alcohol Mixtures: Spherulitic Growth, Polymorph Stabilization, and Morphology Change." Crystal Growth And Design **12**: 842-853.

Sawada, K., Ogino, T., & Suzuki, T. (1990). "The distribution coefficients of Mg^{2+} ion between $CaCO_3$ polymorphs and solution and the effects on the formation and transformation of $CaCO_3$ in water". Journal of Crystal Growth **106**(2): 393-399.

Stoll, H. M., Rosenthal, Y., & Falkowski, P. (2002). "Climate proxies from Sr/Ca of coccolith calcite: calibrations from continuous culture of *Emiliania huxleyi*". Geochimica et Cosmochimica Acta **66**(6): 927-936.

Stoll, H. M., & Schrag, D. P. (1998). "Effects of Quaternary sea level cycles on strontium in seawater." Geochimica et Cosmochimica Acta **62**(7): 1107-1118.

Wanamaker Jr, A. D., Kreutz, K. J., Wilson, T., Borns Jr, H. W., Introne, D. S., & Feindel, S. (2008). "Experimentally determined Mg/Ca and Sr/Ca ratios in juvenile bivalve calcite for *Mytilus edulis*: implications for paleotemperature reconstructions". Geo-Marine Letters **28**(5-6), 359-368.

Wang, D., Wallace, A. F., De Yoreo, J. J., & Dove, P. M. (2009). "Carboxylated molecules regulate magnesium content of amorphous calcium carbonates during calcification". Proceedings of the National Academy of Sciences **106**(51): 21511-21516.

Wang, D., Hamm, L. M., Bodnar, R. J., & Dove, P. M. (2012). "Raman spectroscopic characterization of the magnesium content in amorphous calcium carbonates". Journal of Raman Spectroscopy **43**(4): 543-548.

Wansard, G., De Deckker, P., & Julià, R. (1998). "Variability in ostracod partition coefficients *D*(Sr) and *D*(Mg): Implications for lacustrine palaeoenvironmental reconstructions". Chemical Geology **146**(1): 39-54.

Wasylenki, L. E., Dove, P. M., Wilson, D. S., De Yoreo, J. J. (2005). "Nanoscale effects of strontium on calcite growth: An in situ AFM study in the absence of vital effects." Geochimica et Cosmochimica Acta **69**(12): 3017-3027.

Weber, J. N., & Raup, D. M. (1966). "Fractionation of the stable isotopes of carbon and oxygen in marine calcareous organisms — the Echinoidea". Geochimica et Cosmochimica Acta **30**(7): 681-703.

Weiner, S., Sagi, I., & Addadi, L. (2005). "Choosing the crystallization path less traveled". Science **309**(5737): 1027-1028.

Weiss, I. M., Tuross, N., Addadi, L., & Weiner, S. (2002). "Mollusc larval shell formation: amorphous calcium carbonate is a precursor phase for aragonite". Journal of Experimental Zoology **293**(5): 478-491.

Winland, H. D. (1969). "Stability of calcium carbonate polymorphs in warm, shallow seawater". Journal of Sedimentary Research **39**(4).

Ziegler, A. (1997). "Ultrastructural changes of the anterior and posterior sternal integument of the terrestrial isopod *Porcellio scaber* Latr.(*Crustacea*) during the moult cycle". Tissue and Cell **29**(1): 63-76.

Appendix A: Summary of data showing the pH and transformation times collected for the various temperature experiments.

T (°C)	[Sr] (mM)	ACC pH	Transformation time	Calcite pH
18	0.1	8.08	48 hours	7.52
18	0.5	8.09	48 hours	7.49
18	1.0	8.07	48 hours	7.47
22	0.1	8.10	36 hours	7.50
22	0.5	8.09	36 hours	7.50
22	1.0	8.07	36 hours	7.46
25	0.1	8.03	24 hours	7.50
25	0.5	8.09	24 hours	7.49
25	1.0	8.08	24 hours	7.46
30	0.1	8.07	18 hours	7.49
30	0.5	8.08	18 hours	7.46
30	1.0	8.09	18 hours	7.47

Appendix B: Summary of data showing the ACC Sr/Ca ratios collected for the Mg/Ca ratio batch reactor and flow-through experiments.

Table 1: Batch reaction at 25°C.

Mg:Ca ratio	[Sr] (mM)	Sr/Ca (2 min)	Sr/Ca (45 min)
1:1	0.1	0.0037	0.0036
1:1	0.5	0.016	0.016
1:1	1.0	0.032	0.032
2:1	0.1	0.0031	0.0032
2:1	0.5	0.015	0.015
2:1	1.0	0.030	0.030
5:1	0.1	0.0028	0.0028
5:1	0.5	0.014	0.014
5:1	1.0	0.025	0.027

Table 2: Flow-through reaction at 25°C

Mg:Ca ratio	[Sr] (mM)	Sr/Ca
1:1	0.1	0.0036
1:1	0.5	0.017
1:1	1	0.033
2:1	0.1	0.0041
2:1	0.5	0.016
2:1	1	0.033
5:1	0.1	0.0039
5:1	0.5	0.015
5:1	1	0.029

Appendix C: Summary of raw data showing the Mg/Ca ratios, Sr/Ca ratios and mol percent $MgCO_3$ and $SrCO_3$ calculations collected for the various batch reactor temperature experiments. Each experiment was conducted with 25 mM $CaCl_2$ and 125 mM $MgCl_2$ (Mg/Ca = 5/1).

Table 1: Batch reaction at 18°C.

$[Sr]^o$ (mM)	Phase	[Ca] (mM)	[Mg] (mM)	[Sr] (mM)	Mg/Ca	Sr/Ca	mol% $MgCO_3$	mol% $SrCO_3$
0.1	Aqueous (2 min)	16.99	155.31	0.11	9.14	0.006	90.08	0.06
0.1	Aqueous (45 min)	11.99	115.28	0.08	9.61	0.007	90.52	0.06
0.1	Aqueous (calcite)	6.91	116.80	0.06	16.91	0.008	94.37	0.05
0.1	ACC (2 min)	18.58	7.38	0.07	0.40	0.004	28.36	0.27
0.1	ACC (45 min)	2.54	1.29	0.01	0.51	0.004	33.57	0.25
0.1	Calcite	29.07	8.60	0.11	0.30	0.004	22.77	0.30
0.5	Aqueous (2 min)	17.73	153.15	0.43	8.64	0.024	89.40	0.25
0.5	Aqueous (45 min)	11.87	106.11	0.29	8.94	0.024	89.72	0.25
0.5	Aqueous (calcite)	6.06	102.26	0.20	16.88	0.033	94.24	0.18
0.5	ACC (2 min)	9.78	3.67	0.13	0.38	0.013	27.02	0.97
0.5	ACC (45 min)	1.83	1.01	0.03	0.55	0.014	35.29	0.89
0.5	Calcite	22.50	6.28	0.31	0.28	0.014	21.58	1.06
1.0	Aqueous (2 min)	13.25	114.68	0.64	8.65	0.049	89.19	0.50
1.0	Aqueous (45 min)	12.05	108.15	0.59	8.98	0.049	89.54	0.49
1.0	Aqueous (calcite)	7.76	113.54	0.49	14.64	0.064	93.23	0.41
1.0	ACC (2 min)	5.29	2.34	0.14	0.44	0.026	30.13	1.76
1.0	ACC (45 min)	2.39	1.24	0.07	0.52	0.028	33.49	1.81
1.0	Calcite	25.78	7.36	0.66	0.29	0.026	21.78	1.96

Table 2: Batch reaction at 22°C.

[Sr] (mM)	Phase	[Ca] (mM)	[Mg] (mM)	[Sr] (mM)	Mg/Ca	Sr/Ca	mol% $MgCO_3$	mol% $SrCO_3$
0.1	Aqueous (2 min)	12.31	106.83	0.06	8.68	0.005	89.63	0.05
0.1	Aqueous (45 min)	13.19	111.88	0.06	8.48	0.005	89.41	0.05
0.1	Aqueous (calcite)	7.65	110.02	0.05	14.37	0.006	93.46	0.04
0.1	ACC (2 min)	6.07	2.45	0.02	0.40	0.003	28.70	0.21
0.1	ACC (45 min)	3.50	1.72	0.01	0.49	0.003	32.97	0.20
0.1	Calcite	32.99	10.18	0.09	0.31	0.003	23.54	0.21
0.5	Aqueous (2 min)	11.56	111.29	0.30	9.63	0.026	90.37	0.24
0.5	Aqueous (45 min)	10.63	105.55	0.28	9.93	0.026	90.64	0.24
0.5	Aqueous (calcite)	8.78	111.23	0.26	12.67	0.030	92.48	0.22
0.5	ACC (2 min)	7.70	3.42	0.11	0.44	0.014	30.45	0.98
0.5	ACC (45 min)	5.58	2.67	0.08	0.48	0.014	32.08	0.96
0.5	Calcite	32.62	10.87	0.44	0.33	0.014	24.74	1.00
1.0	Aqueous (2 min)	12.50	116.01	0.60	9.28	0.048	89.85	0.46
1.0	Aqueous (45 min)	11.66	112.98	0.58	9.69	0.050	90.22	0.46
1.0	Aqueous (calcite)	10.46	115.70	0.57	11.06	0.055	91.29	0.45
1.0	ACC (2 min)	8.99	4.37	0.26	0.49	0.029	32.11	1.88
1.0	ACC (45 min)	14.45	6.36	0.40	0.44	0.028	30.00	1.87
1.0	Calcite	14.99	4.90	0.40	0.33	0.027	24.15	1.97

Table 3: Batch reaction at 25°C

[Sr] (mM)	Phase	[Ca] (mM)	[Mg] (mM)	[Sr] (mM)	Mg/Ca	Sr/Ca	mol% $MgCO_3$	mol% $SrCO_3$
0.1	Aqueous (2 min)	14.59	122.31	0.08	8.39	0.006	89.29	0.06
0.1	Aqueous (45 min)	12.08	106.56	0.07	8.82	0.006	89.77	0.06
0.1	Aqueous (calcite)	10.00	119.28	0.07	11.93	0.007	92.22	0.05
0.1	ACC (2 min)	2.83	1.86	0.01	0.66	0.003	39.53	0.20
0.1	ACC (45 min)	3.56	2.15	0.01	0.60	0.003	37.61	0.21
0.1	Calcite	27.27	8.47	0.09	0.31	0.003	23.63	0.24
0.5	Aqueous (2 min)	12.60	106.28	0.31	8.43	0.025	89.17	0.26
0.5	Aqueous (45 min)	12.43	109.99	0.31	8.85	0.025	89.62	0.25
0.5	Aqueous (calcite)	11.02	119.84	0.31	10.87	0.028	91.36	0.23
0.5	ACC (2 min)	4.01	2.10	0.06	0.52	0.014	34.10	0.92
0.5	ACC (45 min)	5.23	2.64	0.08	0.50	0.014	33.21	0.95
0.5	Calcite	18.09	5.75	0.25	0.32	0.014	23.87	1.02
1.0	Aqueous (2 min)	15.10	128.76	0.75	8.53	0.050	89.04	0.52
1.0	Aqueous (45 min)	13.61	121.69	0.69	8.94	0.051	89.48	0.51
1.0	Aqueous (calcite)	12.12	123.95	0.68	10.23	0.056	90.64	0.49
1.0	ACC (2 min)	5.26	2.62	0.14	0.50	0.026	32.63	1.74
1.0	ACC (45 min)	6.77	3.44	0.18	0.51	0.027	33.08	1.76
1.0	Calcite	17.99	5.45	0.48	0.30	0.026	22.79	1.99

Table 4: Batch reaction at 30°C.

[Sr] (mM)	Phase	[Ca] (mM)	[Mg] (mM)	[Sr] (mM)	Mg/Ca	Sr/Ca	mol% $MgCO_3$	mol% $SrCO_3$
0.1	Aqueous (2 min)	16.70	113.31	0.08	6.79	0.005	87.10	0.06
0.1	Aqueous (45 min)	14.96	104.56	0.07	6.99	0.005	87.44	0.06
0.1	Aqueous (calcite)	7.18	107.58	0.04	14.98	0.006	93.71	0.04
0.1	ACC (2 min)	2.67	1.16	0.01	0.44	0.003	30.32	0.19
0.1	ACC (45 min)	3.05	1.33	0.01	0.44	0.003	30.31	0.19
0.1	Calcite	33.27	7.11	0.10	0.21	0.003	17.57	0.26
0.5	Aqueous (2 min)	13.84	110.25	0.35	7.96	0.025	88.60	0.28
0.5	Aqueous (45 min)	12.59	104.30	0.32	8.29	0.025	88.99	0.27
0.5	Aqueous (calcite)	7.46	105.69	0.24	14.17	0.032	93.21	0.21
0.5	ACC (2 min)	2.50	1.39	0.03	0.56	0.014	35.38	0.88
0.5	ACC (45 min)	2.39	1.35	0.03	0.56	0.014	35.77	0.90
0.5	Calcite	19.58	5.98	0.28	0.31	0.015	23.13	1.10
1.0	Aqueous (2 min)	8.71	98.53	0.46	11.31	0.053	91.49	0.43
1.0	Aqueous (45 min)	8.19	97.19	0.43	11.87	0.053	91.85	0.41
1.0	Aqueous (calcite)	5.70	97.02	0.38	17.03	0.067	94.10	0.37
1.0	ACC (2 min)	4.08	2.52	0.13	0.62	0.032	37.44	1.92
1.0	ACC (45 min)	2.51	1.79	0.08	0.71	0.032	40.81	1.85
1.0	Calcite	32.85	15.04	0.98	0.46	0.030	30.77	2.00